Attenuation of flexural phonons in free-standing crystalline two-dimensional materials

A. D. Kokovin [1,2] and I. S. Burmistrov [2,3]
[1]*Moscow Institute for Physics and Technology, 141700 Moscow, Russia*
[2]*L. D. Landau Institute for Theoretical Physics, 142432 Chernogolovka, Russia*
[3]*Laboratory for Condensed Matter Physics, National Research University Higher School of Economics, 101000 Moscow, Russia*

(Received 7 December 2023; accepted 22 February 2024; published 27 September 2024)

We develop the theory for dynamics of the out-of-plane deformations in flexible two-dimensional materials. We focus on study of attenuation of flexural phonons in free-standing crystalline membranes. We demonstrate that the dynamical renormalization does not involve the ultraviolet divergent logarithmic contributions contrary to the static ones. This fact allows us to find the scaling form of the attenuation, determine its small- and large-frequency asymptotes, and to derive the exact expression for the dynamical exponent of flexural phonons in the long-wave limit: $\mathsf{z} = 2 - \eta/2$. Here η is the universal exponent controlling the static renormalization of the bending rigidity. Also we determine the dynamical exponent for the long-wave in-plane phonons: $\mathsf{z}' = (2 - \eta/2)/(1 + \eta/2)$. We discuss implication of our results to experiments on phonon spectra in graphene and dynamics of graphene-based nanomechanical resonators.

DOI: 10.1103/PhysRevB.110.125432

I. INTRODUCTION

Following the discovery of graphene [1–3] and other atomically thin materials [4], flexible two-dimensional (2D) materials [5] have been attracting a lot of theoretical and experimental interest. These materials, the so-called crystalline membranes, have a peculiar elastic properties dubbed as anomalous elasticity. The latter includes nontrivial scaling of elastic modules with the system size, crumpling transition with increasing temperature and disorder, nonlinear Hooke's law, negative Poisson ratios, etc. [6–21]. Currently there has been substantial progress in further theoretical understanding of static properties of crystalline membranes [22–41].

Contrary to extensive study of thermodynamics of membranes, there are just a few works (at least to our knowledge) devoted to membrane's dynamics. The renormalization group method developed to study the static elastic properties of $D = 4 - \epsilon$-dimensional membranes (with $\epsilon \ll 1$) has been extended to investigate dynamical exponent for out-of-plane and in-plane phonons [42]. The dynamics of 2D membranes has recently been studied within phenomenological Langevin-type approach [43–46]. Intriguingly, the dynamical exponents predicted in both above-mentioned approaches differ from each other. To resolve the issue, the microscopic theory for the attenuation of flexural phonons in 2D crystalline materials is needed to be developed. One more motivation for such a theory comes from recent measurement of the phonon spectrum in graphene by the method of the high-resolution electron energy loss spectroscopy [47].

A detailed theory for the attenuation of flexural phonons (due to nonlinear effects induced by coupling between in-plane and out-of-plane displacements) is not only of an academic interest. Graphene and other 2D crystalline materials are intensively explored as nanoelectromechanical systems with relatively high-quality factors [48,49] (see Refs. [50,51] for a review). Also a real-time height dynamics of a free-standing graphene membrane has recently been monitored [52]. Although there could be many microscopic sources for damping of graphene mechanical nanoresonators [53], the flexural phonon decay is unavoidable source for intrinsic contribution to damping.

In this paper, we develop the comprehensive theory of the decay time (τ_k) of out-of-plane phonons in free-standing 2D crystalline membranes. We focus on an experimentally relevant temperature range in which flexural phonons can be treated classically, $k_B T \gg \hbar\omega_k$. We establish an unexpected result that the decay rate of long-wave flexural phonons is independent of temperature and is of the order of the phonon frequency, $1/\tau_k \sim \omega_k$. Also we determine exactly the dynamical exponent for the long-wave flexural phonons: $\omega_k \sim k^{\mathsf{z}}$, $\mathsf{z} = 2 - \eta/2$, cf. Eq. (62). Here k denotes the phonon momentum and η is the universal exponent controlling the static renormalization of the bending rigidity. Also we derive similar relation for the spectrum of in-plane phonons with the corresponding dynamical exponent $\mathsf{z}' = (2 - \eta/2)/(1 + \eta/2)$. As application of our results we compute the time-dependent pair correlation function of membrane's height, cf. Eq. (63).

The outline of the paper is as follows. In Sec. II we formulate the model of elastic deformations of 2D membrane and announce our main results. In Sec. III we remind a reader the results for the static renormalization of the theory. The computation of the flexural phonon attenuation is presented in Sec. IV. We explain why there is no effect of dynamics on the crumpling transition in Sec. V. In Sec. VI we compute the time dependence of pair correlation function of out-of-plane displacement. We end the paper with discussions and conclusions (Sec. VII). Details of computations are relegated to the Appendices. Throughout the paper we use unites with $k_B = \hbar = 1$.

II. MODEL AND MAIN RESULTS

The theory of elasticity of clean 2D crystalline membranes embedded in $d = 3$-dimensional space is given by the

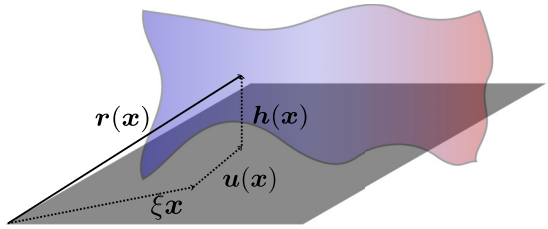

FIG. 1. A sketch of rippled membrane with dynamical fluctuations (colored) and reference plane (gray).

following free energy [6–8]:

$$\mathcal{F} = \int d^2\boldsymbol{x}\left[\frac{\varkappa}{2}(\Delta \boldsymbol{r})^2 + \mu u_{\alpha\beta}u_{\alpha\beta} + \frac{\lambda}{2}u_{\alpha\alpha}^2\right]. \tag{1}$$

Here $\boldsymbol{x}$ is the $d = 2$ coordinate vector of a point on the reference plane while $\boldsymbol{r}$ denotes a $d = 3$-dimensional vector parametrizing a point on the membrane (see Fig. 1). We introduced the deformation tensor $u_{\alpha\beta} = (\partial_\alpha \boldsymbol{r}\partial_\beta \boldsymbol{r} - \delta_{\alpha\beta})/2$, with $\alpha, \beta = x, y$. The bending rigidity is denoted by $\varkappa$ while λ and μ are Lamé coefficients.

In order to describe the membrane which is not close to the crumpling transition, it is convenient to separate homogeneous stretching (ξ) of the membrane, parametrizing the 3D vector $\boldsymbol{r}$ as

$$r_1 = \xi x + u_x, \quad r_2 = \xi y + u_y, \quad r_3 = h. \tag{2}$$

Then the deformation tensor acquires the following form $u_{\alpha\beta} = (\xi^2 - 1)\delta_{\alpha\beta}/2 + \tilde{u}_{\alpha\beta}$, where (no summation over repeating indices is assumed)

$$\tilde{u}_{\alpha\beta} = \tfrac{1}{2}(\xi_\beta \partial_\alpha u_\beta + \xi_\alpha \partial_\beta u_\alpha + \partial_\alpha h \partial_\beta h + \partial_\alpha \boldsymbol{u}\partial_\beta \boldsymbol{u}). \tag{3}$$

An inhomogeneous deformation of the membrane is characterized by the $d = 2$ in-plane displacement vector $\boldsymbol{u} = \{u_x, u_y\}$ and the scalar out-of-plane deformation h.

In order to study dynamics of the in-plane and out-of-plane fluctuations we will work within the path integral formulation in the imaginary time. The partition function is given as

$$Z = \int \mathcal{D}[h, \boldsymbol{u}] \exp\left[-\int_0^\beta d\tau\left(\frac{\rho}{2}\int d^2\boldsymbol{x}\,(\partial_\tau \boldsymbol{r})^2 + \mathcal{F}\right)\right]. \tag{4}$$

Here $\beta = 1/T$ is the inverse temperature and ρ is the mass density of the membrane.

Provided the membrane is in the flat phase away from the crumpling transition, it is legitimate [6] to omit the term $\partial_\alpha \boldsymbol{u}\partial_\beta \boldsymbol{u}$ in Eq. (3). Similarly, one can neglect the contribution from $\boldsymbol{u}$ to the bending energy. Then the free energy Eq. (1) becomes quadratic in terms of the in-plane displacements. It allows us to integrate over $\boldsymbol{u}$ in Eq. (4) exactly and to derive the effective action for the out-of-plane displacement alone (see details of derivation in Refs. [23,25]),

$$Z = \int \mathcal{D}[h] e^{-S}, \quad S = S_0 + S_{\rm dyn}, \tag{5}$$

where

$$S_0 = \frac{\beta}{8}\int d^2\boldsymbol{x}\, c_{\alpha\beta}\varepsilon_\alpha\varepsilon_\beta, \quad \varepsilon_\alpha = \xi^2 - 1 + \sum_{\omega,\boldsymbol{k}} k_\alpha^2 |h_{\boldsymbol{k},\omega}|^2, \tag{6}$$

and

$$S_{\rm dyn} = \frac{1}{2}\sum_{\omega,\boldsymbol{k}}(\varkappa k^4 + \rho\omega^2)|h_{\boldsymbol{k},\omega}|^2 + \frac{Y}{8}\sum_{\Omega,\boldsymbol{q}\neq 0}\left|\sum_{\omega,\boldsymbol{k}}\frac{[\boldsymbol{k}\times\boldsymbol{q}]^2}{q^2}h_{\boldsymbol{k}+\boldsymbol{q},\omega+\Omega}h_{-\boldsymbol{k},-\Omega}\right|^2. \tag{7}$$

Here $c_{\alpha\beta} = \lambda + 2\mu\delta_{\alpha\beta}$ denotes the matrix of elastic stiffness constants and $Y = 4\mu(\mu+\lambda)/(2\mu+\lambda)$ is the Young's modulus. Also we performed the Fourier transform

$$h(\boldsymbol{x}, \tau) = \sum_{\omega_n,\boldsymbol{k}} h_{\boldsymbol{k},\omega_n} e^{i(\boldsymbol{k}\boldsymbol{x} - \omega_n\tau)}, \tag{8}$$

where $\omega_n = 2\pi T n$ are the bosonic Matsubara frequencies. Here and in what follows, we use the short-hand notation $\sum_{\omega_n,\boldsymbol{k}} = T\sum_{\omega_n}\int d^2k/(2\pi)^2$. We note that the term $\sum_{\omega,\boldsymbol{k}} k_\alpha^2|h_{\boldsymbol{k},\omega}|^2$ in the displacement ε_α is responsible for the anomalous Hooke's law.

Generally, due to dynamics of the in-plane phonons, the interaction in the second line of Eq. (7), i.e., the Young's modulus Y, depends on the transferred frequency Ω, see Ref. [25]. However, as one can check, the static limit of interaction mediated by the in-plane phonons is enough for our computations (see Appendix A for details).

The quadratic part of action (7) determines the "bare" Green's function in the Matsubara representation,

$$G_{\boldsymbol{k}}(i\omega) = \frac{1}{\rho\omega^2 + \varkappa k^4}. \tag{9}$$

The corresponding retarded and advanced Green's functions are given as

$$G_{\boldsymbol{k}}^{R/A}(\omega) = -\frac{1}{\rho(\omega \pm i0^+)^2 - \varkappa k^4}. \tag{10}$$

Using Eq. (10) one can extract the spectrum of noninteracting flexural phonons:

$$\omega_k^{(0)} = Dk^2, \qquad D = \sqrt{\varkappa/\rho}. \tag{11}$$

Since the theory (7) is interacting, the exact Green's function is related with the bare one by the Dyson equation

$$\mathcal{G}_{\boldsymbol{k}}^{-1}(i\omega) = G_{\boldsymbol{k}}^{-1}(i\omega) - \Sigma_{\boldsymbol{k}}(i\omega),$$
$$\left[\mathcal{G}_{\boldsymbol{k}}^{R/A}(\omega)\right]^{-1} = \left[G_{\boldsymbol{k}}^{R/A}(\omega)\right]^{-1} - \Sigma_{\boldsymbol{k}}^{R/A}(\omega). \tag{12}$$

In this paper our aim is to compute the frequency dependence of the retarded self-energy $\Sigma_{\boldsymbol{k}}^R(\omega)$. As usual, it is related with $\Sigma_{\boldsymbol{k}}(i\omega)$ by analytic continuation $i\omega \to \omega + i0^+$. The static self-energy $\Sigma_{\boldsymbol{k}}^R(0)$ was studied in many works before. It is well established that the perturbation theory in powers of interaction produces ultraviolet logarithmic divergences that can be summed by means of the renormalization group (RG). The emergent ultraviolet scale is the so-called inverse Ginzburg length, $q_* = \sqrt{3YT/(32\pi\varkappa^2)}$. Such RG-improved perturbation theory results in a power-law renormalization of the bending rigidity and Young's modulus [7,9],

$$\varkappa(k) = \varkappa(q_*/k)^\eta, \quad Y(k) = Y(q_*/k)^{2-2\eta}, \quad k \ll q_*, \tag{13}$$

where the universal exponent $\eta \simeq 0.795 \pm 0.01$ is determined numerically [54].

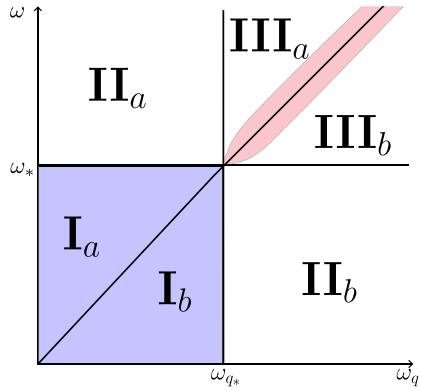

FIG. 2. A sketch of the range of momenta and frequencies ω considered in the paper. The horizontal axis represents the frequency ω_q corresponding to the momentum q: $\omega_q = Dq^2(q/q_*)^{-\eta/2}$ for $q < q_*$ and $\omega_q = Dq^2$ for $q > q_*$.

It is convenient to introduce the frequency scale corresponding to the Ginzburg length, $\omega_* = Dq_*^2$. Introducing the dimensionless parameter characterizing the strength of quantum effects for membrane, $g = 21Y/(128\pi\sqrt{\rho\varkappa^3})$ [22,24,25], we find that $\omega_* = (4/7)gT$. In what follows we will assume that $g \ll 1$ (e.g., for graphene $g \approx 0.05$). Also we will consider the following range of momenta and frequencies, see Fig. 2:

$$k \ll q_*, \quad |\omega| \ll \omega_* \ll T. \tag{14}$$

Below we will call the regime (14) as the universal regime.

We demonstrate below that the retarded self-energy in the range (14) can be written in the following scaling form:

$$\begin{aligned} \mathrm{Re}\,\Sigma^R_{\boldsymbol{k}}(\omega) - \Sigma^R_{\boldsymbol{k}}(0) &= \rho\omega_k^2 \mathcal{F}_1(\omega/\omega_k), \\ \mathrm{Im}\,\Sigma^R_{\boldsymbol{k}}(\omega) &= \rho\omega\omega_k \mathcal{F}_2(\omega/\omega_k). \end{aligned} \tag{15}$$

This is the main result of our work. Here we introduce

$$\omega_k = Dk^2(k/q_*)^{-\eta/2} \sim k^{\mathsf{z}}, \quad \mathsf{z} = 2 - \eta/2, \tag{16}$$

that is up to an unknown numerical factor describes the exact spectrum of a flexural phonon. The scaling functions $\mathcal{F}_1(z)$ and $\mathcal{F}_2(z)$ are even functions of their argument, satisfy the normalization condition $\mathcal{F}_1(0) = 0$, and obey Kramers-Kronig-type relations,

$$\begin{aligned} \mathcal{F}_1(z) &= \mathrm{p.v.}\int_{-\infty}^{\infty} \frac{dx}{\pi}\frac{z\mathcal{F}_2(x)}{x-z}, \\ \mathcal{F}_2(z) &= \mathrm{p.v.}\int_{-\infty}^{\infty} \frac{dx}{\pi}\frac{\mathcal{F}_1(x)}{z(z-x)}. \end{aligned} \tag{17}$$

The qualitative behavior of functions $\mathcal{F}_1(z)$ and $\mathcal{F}_2(z)$ is shown in Fig. 3.

The relations (15) implies the following scaling form of the exact retarded Green's function:

$$\mathcal{G}^R_{\boldsymbol{k}}(\omega) = -\frac{1}{\rho}\left[\omega^2 - \omega_k^2\left[1 - \mathcal{F}_1\left(\frac{\omega}{\omega_k}\right)\right] + i\omega\omega_k\mathcal{F}_2\left(\frac{\omega}{\omega_k}\right)\right]^{-1}. \tag{18}$$

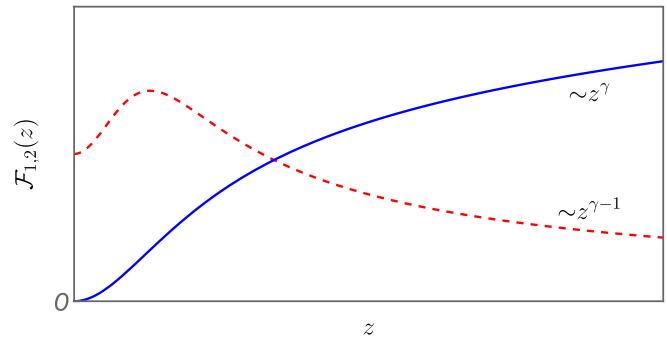

FIG. 3. The sketch of the behavior of the functions $\mathcal{F}_1(z)$ (blue solid curve) and $\mathcal{F}_2(z)$ (red dashed curve). The exponent γ is defined in (32).

In the next two sections, Secs. III and IV, we will explain how the results (15) can be derived and present asymptotic expressions for the functions $\mathcal{F}_{1,2}$. Physical implications of the result (18) are discussed in Secs. V and VI.

III. STATIC RENORMALIZATION

The theory of static out-of-plane displacements was extensively explored previously (see Ref. [28] for a review). In this section, we remind a reader how these results, in particular, Eq. (13), can be derived within frequency-dependent Green's functions.

Let us start from the self-energy contribution shown in Fig. 4,

$$\Sigma^{(1)}_{\boldsymbol{k}}(i\omega) = -2\sum_{\Omega,\boldsymbol{q}} \frac{[\boldsymbol{k}\times\boldsymbol{q}]^4}{q^4} N_{\boldsymbol{q}}(i\Omega) G_{\boldsymbol{k}+\boldsymbol{q}}(i\omega + i\Omega). \tag{19}$$

It is the first-order correction to the self-energy in the dynamically screened interaction computed within random phase approximation (RPA) (see Fig. 4),

$$N_{\boldsymbol{q}}(i\Omega) = \frac{Y/2}{1 + 3Y\,\Pi^{(0)}_{\boldsymbol{q}}(i\Omega)/2}. \tag{20}$$

Here the "bare" polarization operator is given as

$$\Pi^{(0)}_{\boldsymbol{q}}(i\Omega) = \frac{1}{3}\sum_{\omega,\boldsymbol{k}} \frac{[\boldsymbol{k}\times\boldsymbol{q}]^4}{q^4} G_{\boldsymbol{k}}(i\omega) G_{\boldsymbol{k}+\boldsymbol{q}}(i\omega + i\Omega). \tag{21}$$

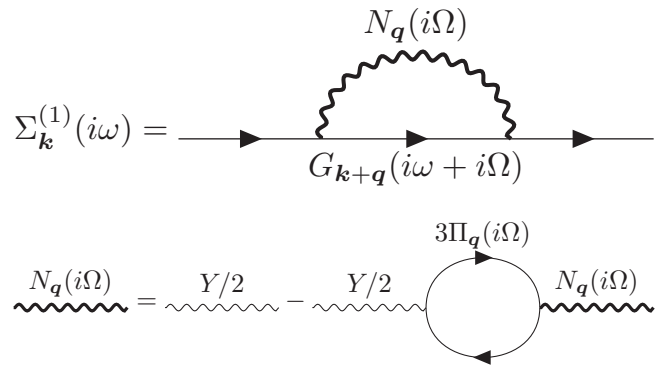

FIG. 4. Top: SCSA-like contribution to the self-energy correction. Bottom: RPA-like screened interaction.

We emphasize that RPA-type screening is crucial in the region $q \ll q_*$ since $Y\Pi_q^{(0)}(0) \sim (q_*/q)^2 \gg 1$. Making the analytic continuation in Eq. (19) to the real frequencies, $i\omega \to \omega + i0$, we find

$$\Sigma_{\boldsymbol{k}}^{(1),R}(\omega) = -\int \frac{d\Omega}{\pi} \int \frac{d^2\boldsymbol{q}}{(2\pi)^2} \frac{[\boldsymbol{k}\times\boldsymbol{q}]^4}{q^4} \left[\coth\frac{\Omega}{2T} \mathrm{Im} N_{\boldsymbol{q}}^R(\Omega) G_{\boldsymbol{k}+\boldsymbol{q}}^R(\omega+\Omega) + \coth\frac{\omega+\Omega}{2T} N_{\boldsymbol{q}}^A(\Omega) \mathrm{Im} G_{\boldsymbol{k}+\boldsymbol{q}}^R(\omega+\Omega) \right]. \tag{22}$$

Here we introduced retarded dynamically screened interaction, $N_{\boldsymbol{q}}^R(\Omega) = (Y/2)/[1+3Y\Pi_{\boldsymbol{q}}^{(0),R}(\Omega)/2]$, where

$$\Pi_{\boldsymbol{q}}^{(0),R}(\Omega) = \int \frac{d\omega}{2\pi} \int \frac{d^2\boldsymbol{k}}{(2\pi)^2} \frac{[\boldsymbol{k}\times\boldsymbol{q}]^4}{3q^4} \left\{ \coth\frac{\omega}{2T} \mathrm{Im} G_{\boldsymbol{k}}^R(\omega) G_{\boldsymbol{k}+\boldsymbol{q}}^R(\omega+\Omega) + \coth\frac{\omega+\Omega}{2T} G_{\boldsymbol{k}}^A(\omega) \mathrm{Im} G_{\boldsymbol{k}+\boldsymbol{q}}^R(\omega+\Omega) \right\}. \tag{23}$$

is the retarded polarization operator corresponding to the Matsubara one, cf. Eq. (21). We note that $N_{\boldsymbol{q}}^A(\Omega)$ can be obtained from $N_{\boldsymbol{q}}^R(\Omega)$ by complex conjugation.

Setting in Eq. (19) the frequency ω to zero, we obtain

$$\mathrm{Re}\Sigma_{\boldsymbol{k}}^{(1),R}(0) = -\int \frac{d\Omega}{\pi} \coth\frac{\Omega}{2T} \int \frac{d^2\boldsymbol{q}}{(2\pi)^2} \frac{[\boldsymbol{k}\times\boldsymbol{q}]^4}{q^4} \times \mathrm{Im}\left[N_{\boldsymbol{q}}^R(\Omega) G_{\boldsymbol{k}+\boldsymbol{q}}^R(\Omega)\right]. \tag{24}$$

In the classical regime, $T \gg |\Omega|$ we can use the following approximation: $\coth(\Omega/2T) \sim 2T/\Omega$. Then we perform the integral over Ω in Eq. (24) with the help of Kramers-Kronig relation. Eventually, we find

$$\mathrm{Re}\Sigma_{\boldsymbol{k}}^{(1),R}(0) = -2T \int \frac{d^2\boldsymbol{q}}{(2\pi)^2} \frac{[\boldsymbol{k}\times\boldsymbol{q}]^4}{q^4} N_{\boldsymbol{q}}^R(0) G_{\boldsymbol{k}+\boldsymbol{q}}^R(0). \tag{25}$$

Comparison of Eq. (25) with Eq. (19) shows that Eq. (25) fully reproduces the result of static treatment.

A similar procedure can be performed for all other diagrams as well. For example, for the diagram shown in Fig. 5 we find (see Appendix B):

$$\mathrm{Re}\Sigma_{\boldsymbol{k}}^{(2),R}(0) = -4T^2 \sum_{\boldsymbol{q},\boldsymbol{Q}} \frac{[(\boldsymbol{k}+\boldsymbol{Q})\times\boldsymbol{q}]^2}{q^2} \frac{[(\boldsymbol{k}+\boldsymbol{q})\times\boldsymbol{Q}]^2}{Q^2} \frac{[\boldsymbol{k}\times\boldsymbol{q}]^2}{q^2} \times \frac{[\boldsymbol{k}\times\boldsymbol{Q}]^2}{Q^2} G_{\boldsymbol{k}+\boldsymbol{q}}^R(0) G_{\boldsymbol{k}+\boldsymbol{Q}}^R(0) \times G_{\boldsymbol{k}+\boldsymbol{q}+\boldsymbol{Q}}^R(0) N_{\boldsymbol{q}}^R(0) N_{\boldsymbol{Q}}^R(0). \tag{26}$$

The analysis above can be extended to any self-energy diagram with zero external frequency. Indeed, only the static Green's function and static screened interaction contribute to the zero-frequency self-energy corrections in the classical regime, $\omega \ll T$.

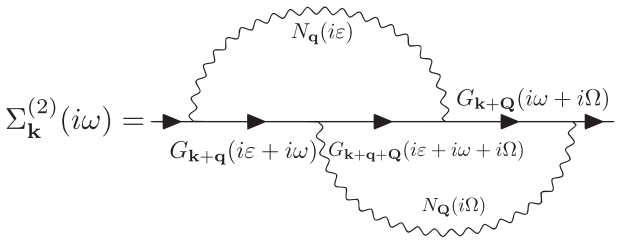

FIG. 5. Non-SCSA-like contribution to the self-energy correction.

As we discussed above, the diagrams for static self-energy are logarithmically divergent and q_* serves as the ultraviolet cutoff. Therefore, it is worthwhile, at first, to sum up all contributions to $\Sigma_{\boldsymbol{k}}^R(0)$, and only then to develop perturbation theory for $\mathrm{Im}\Sigma_{\boldsymbol{k}}^R(\omega)$ (see discussion of similar approach in Ref. [42]). This idea implies that new "bare" Green's function for such "dynamical" perturbation theory reads

$$\mathcal{G}_{\boldsymbol{k}}^{(0)}(i\omega) = \frac{1}{\rho\omega^2 + \varkappa k^4 - \Sigma_{\boldsymbol{k}}^R(0)} \equiv \frac{1}{\rho\left(\omega^2+\omega_k^2\right)}, \tag{27}$$

where ω_k is given by Eq. (16). We note that the perturbation theory for $\mathrm{Im}\Sigma_{\boldsymbol{k}}(\omega)$ consists of the same diagrams as the one for the full self-energy but, additionally, a number of diagrams to avoid double counting is needed to be considered. We discuss this issue in detail in Appendix C. Although, due to counterterms such a diagrammatic technique is not convenient beyond the lowest order in interaction; nevertheless, it has an important advantage: As we will demonstrate below the diagrams computed with the help of the Green's function with the statically renormalized phonon spectrum, Eq. (27), are convergent in the ultraviolet.

IV. INTERACTION-INDUCED FLEXURAL PHONON DECAY

Now we are ready to compute the imaginary part of the self-energy that determines the decay of flexural phonons. The source of decay is the four-phonon processes, see Fig. 6, due to the interaction term in the second line of Eq. (7).

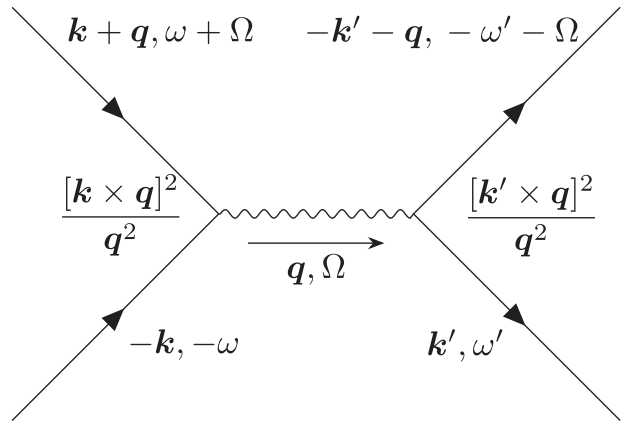

FIG. 6. Diagram illustrating a four-phonon process.

We start from the diagram shown in Fig. 4. Taking the imaginary part of the expression (24), we find the following result in the universal regime (regions I_a and I_b in Fig. 2):

$$\mathrm{Im}\Sigma^{(1),R}_{\boldsymbol{k}}(\omega) = -\frac{2T\omega}{3}\int\frac{d\Omega}{\pi}\int\frac{d^2\boldsymbol{q}}{(2\pi)^2}\frac{[\boldsymbol{k}\times\boldsymbol{q}]^4}{q^4}\frac{\mathrm{Im}\Pi^{(0),R}_{\boldsymbol{q}}(\Omega)}{\left|\Pi^{(0),R}_{\boldsymbol{q}}(\Omega)\right|^2} \times\frac{\mathrm{Im}\mathcal{G}^{(0),R}_{\boldsymbol{k}+\boldsymbol{q}}(\omega+\Omega)}{\Omega(\omega+\Omega)}. \tag{28}$$

Here we substituted G by $\mathcal{G}^{(0)}$. Also the polarization operator $\Pi^R_{\boldsymbol{q}}(\Omega)$ is given by Eq. (23) with the Green's function G substituted by $\mathcal{G}^{(0)}$. Before analyzing the correction (28), we discuss the frequency dependence of the polarization operator.

A. Polarization operator

Taking the imaginary part of the right-hand side of Eq. (23), we obtain the following expression in the universal regime:

$$\mathrm{Im}\Pi^{(0),R}_{\boldsymbol{q}}(\Omega) = \frac{2T\Omega}{3}\int\frac{d\omega}{2\pi}\int\frac{d^2\boldsymbol{k}}{(2\pi)^2}\frac{[\boldsymbol{k}\times\boldsymbol{q}]^4}{q^4}\frac{\mathrm{Im}\mathcal{G}^{(0),R}_{\boldsymbol{k}}(\omega)}{\omega} \times\frac{\mathrm{Im}\mathcal{G}^{(0),R}_{\boldsymbol{k}+\boldsymbol{q}}(\omega+\Omega)}{\omega+\Omega}. \tag{29}$$

Neglecting the external frequency Ω under the integral signs in Eq. (29), we find the following asymptotic behavior at $\Omega\to 0$:

$$\mathrm{Im}\Pi^{(0),R}_{\boldsymbol{q}}(\Omega)\propto\frac{T}{\varkappa^2 q^{2-2\eta}q_*^{2\eta}}\frac{\Omega}{\omega_q},\quad |\Omega|\ll\omega_q. \tag{30}$$

In the opposite case of high frequencies, we obtain

$$\mathrm{Im}\Pi^{(0),R}_{\boldsymbol{q}}(\Omega)\propto\frac{T}{\varkappa^2 q^{2-2\eta}q_*^{2\eta}}\left(\frac{\Omega}{\omega_q}\right)^{-\gamma},\quad |\Omega|\gg\omega_q, \tag{31}$$

where we introduced the exponent

$$\gamma=\frac{1-\eta}{1-\eta/4}\simeq 0.256. \tag{32}$$

The detailed derivation of the above asymptotic results is given in Appendix D.

Equations (30) and (31) together with analytic properties suggest the following form of the polarization operator:

$$\Pi^{(0),R}_{\boldsymbol{q}}(\Omega)=\frac{A_\eta T q_*^{-2\eta}}{\varkappa^2 q^{2-2\eta}}\left[\mathcal{P}^{(0)}_1\left(\frac{\Omega}{\omega_q}\right)+i\mathcal{P}^{(0)}_2\left(\frac{\Omega}{\omega_q}\right)\right]. \tag{33}$$

Here we introduce numerical factor [23]

$$A_\eta=\frac{\Gamma(1+\eta/2)\Gamma(1-\eta)}{2^{5+\eta}\sqrt{\pi}\Gamma^2(2-\eta/2)\Gamma((3+\eta)/2)} \tag{34}$$

to ensure the normalization condition, $\mathcal{P}^{(0)}_1(0)=1$. As it follows from Eqs. (30) and (31), the odd function $\mathcal{P}^{(0)}_2(z)$ has the following asymptotic behavior:

$$\mathcal{P}^{(0)}_2(z)\propto\begin{cases} z, & |z|\ll 1,\\ \mathrm{sgn}z\,|z|^{-\gamma}, & |z|\gg 1.\end{cases} \tag{35}$$

Thus the function $\mathcal{P}^{(0)}_2(z)$ has extrema at $|z|\sim 1$.

In order to determine the asymptotic behavior of the real part of the polarization operator at finite frequency, i.e., the function $\mathcal{P}^{(0)}_1(z)$, we use the Kramers-Kronig relation:

$$\mathcal{P}^{(0)}_1(z)=1+\frac{2z^2}{\pi}\mathrm{p.v.}\int_0^\infty\frac{dy}{y}\frac{\mathcal{P}^{(0)}_2(y)}{y^2-z^2}. \tag{36}$$

Neglecting z under the integral sign in Eq. (36), we find

$$\mathcal{P}^{(0)}_1(z)\simeq 1+\frac{z^2}{\pi}\int_0^\infty\frac{dy}{y}\frac{d}{dy}\frac{\mathcal{P}^{(0)}_2(y)}{y},\quad |z|\ll 1. \tag{37}$$

At large magnitudes of the argument, we obtain (see Appendix D)

$$\mathcal{P}^{(0)}_1(z)\propto z^{-\gamma},\quad |z|\gg 1. \tag{38}$$

We note that at high frequencies, $\Omega\gg\omega_q$, the polarization operator is independent of the momentum, $\Pi^{(0),R}_{\boldsymbol{q}}(\Omega)\sim\Omega^{-\gamma}$. This fact can be naturally understood. One needs to take the static polarization operator and substitute the momentum $q_*(\Omega/\omega_*)^{1/(2-\eta/2)}$ instead of q. The former momentum corresponds to the mass-shell condition, $\Omega=\omega_q$. We note that such situation is consistent with the dynamical exponent $\mathsf{z}=2-\eta/2$ (see more detail in Sec. VI).

B. Result for the first-order self-energy correction

Now we turn back to Eq. (28). With known asymptotic behavior of the polarization operator $\Pi^{(0),R}_{\boldsymbol{q}}(\Omega)$, we are able to show (see Appendix E) that

$$\mathrm{Im}\Sigma^{(1),R}_{\boldsymbol{k}}(\omega)=\rho\omega\omega_k\mathcal{F}^{(1)}_2\left(\frac{\omega}{\omega_k}\right), \tag{39}$$

where the even function $\mathcal{F}^{(1)}_2(z)$ has the following asymptotic behavior:

$$\mathcal{F}^{(1)}_2(z)-\mathcal{F}^{(1)}_2(0)\propto z^2,\quad |z|\ll 1,$$
$$\mathcal{F}^{(1)}_2(z)\propto|z|^{\gamma-1},\quad |z|\gg 1. \tag{40}$$

We emphasize that $\mathrm{Im}\Sigma^{(1),R}_{\boldsymbol{k}}(\omega)$ is given by the ultraviolet convergent integrals and, consequently, it does not involve the frequency scale ω_*.

The real part of the self-energy correction can be parametrized in a similar way as the imaginary one,

$$\mathrm{Re}\Sigma^{(1),R}_{\boldsymbol{k}}(\omega)-\mathrm{Re}\Sigma^{(1),R}_{\boldsymbol{k}}(0)=\rho\omega_k^2\mathcal{F}^{(1)}_1\left(\frac{\omega}{\omega_k}\right). \tag{41}$$

Here the even function $\mathcal{F}^{(1)}_1(z)$ is related with $\mathcal{F}^{(1)}_2(z)$ by Kramers-Kronig-type relation,

$$\mathcal{F}^{(1)}_1(z)=\mathrm{p.v.}\int_{-\infty}^{\infty}\frac{dx}{\pi}\frac{z\mathcal{F}^{(1)}_2(x)}{x-z}. \tag{42}$$

Using asympotics of $\mathcal{F}^{(1)}_2(z)$ we find the following behavior of $\mathcal{F}^{(1)}_1(z)$ at small and large arguments (see Appendix E):

$$\mathcal{F}^{(1)}_1(z)\propto\begin{cases} z^2, & |z|\ll 1,\\ |z|^\gamma, & |z|\gg 1.\end{cases} \tag{43}$$

We emphasize that the frequency integral in the Kramers-Kronig relation (42) is convergent in the ultraviolet such that there is no need in ω_* as ultraviolet cutoff for computation of the function $\mathcal{F}^{(1)}_1(z)$.

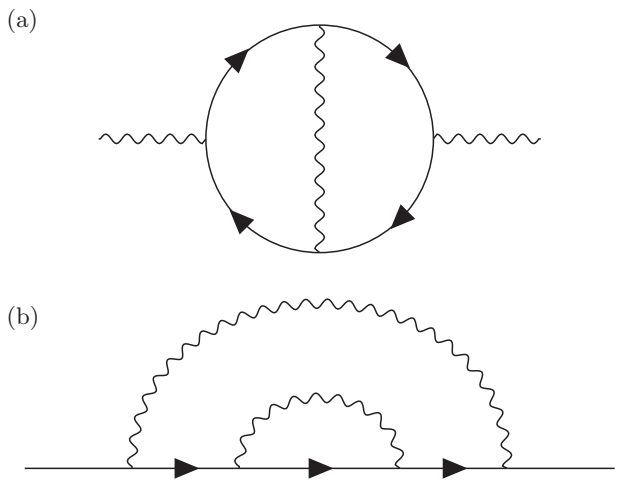

FIG. 7. (a) Correction to the polarization operator. (b) Correction to the self-energy in the next order in the interaction

C. Analysis of higher-order diagrams

In general, there is no reason to limit computation of the dynamical self-energy just by the lowest-order diagram shown in Fig. 4. Moreover, even for that diagram, the polarization operator should be computed in the next orders in the interaction. We show examples of higher-order diagrams in Fig. 7. Although the analytical computation of all necessary diagrams is hopeless, we can compute asymptotic behavior of both the exact polarization operator and the exact self-energy.

Assuming that frequency behavior of the self-energy is the same as given by Eqs. (40) and (43), one can check that the exact polarization operator retains the same scaling form as in Eq. (33) (see Appendix F for details). So we find that the exact polarization operator can be written as

$$\Pi^R_{\boldsymbol{q}}(\Omega) = \frac{T}{\varkappa^2 q^{2-2\eta} q_*^{2\eta}} \left[\mathcal{P}_1\left(\frac{\Omega}{\omega_q}\right) + i\mathcal{P}_2\left(\frac{\Omega}{\omega_q}\right)\right], \tag{44}$$

where $\mathcal{P}_1(z)$ and $\mathcal{P}_2(z)$ are even and odd functions of z, respectively. They have the following asymptotic behavior:

$$\mathcal{P}_1(z) = \mathcal{P}_1(0)\left(1+B_1^{(0)} z^2\right), \quad \mathcal{P}_2(z) = B_2^{(0)} z, \quad |z| \ll 1, \tag{45}$$

and

$$\mathcal{P}_1(z) = B_1^{(\infty)} |z|^{-\gamma}, \quad \mathcal{P}_2(z) = B_2^{(\infty)} \mathrm{sgn} z\, |z|^{-\gamma}, \quad |z| \gg 1, \tag{46}$$

where $B_{1,2}^{(0,\infty)}$ are numerical coefficients. We note that we do not normalize $\mathcal{P}_1(0)$ to be equal to unity. In virtue of the Kramers-Kronig relations we find relations the numerical coefficients introduced above have to satisfy,

$$\mathcal{P}_1(0) = \frac{2}{\pi}\int_0^\infty \frac{dx}{x}\mathcal{P}_2(x), \quad B_1^{(0)} = \frac{\int_0^\infty dx\, \mathcal{P}_2''(x)/x}{\int_0^\infty dx\, \mathcal{P}_2(x)/(2x)} \tag{47}$$

and

$$B_1^{(\infty)} = -B_2^{(\infty)}\Phi_\gamma, \quad \Phi_\gamma = \int_0^\infty \frac{dt}{\pi t}[(1+t)^\gamma - |1-t|^\gamma]. \tag{48}$$

Now we can use the results (44)–(46) in order to compute higher-order diagrams for the self-energy whose examples are shown in Fig. 7. Then for the exact Green's function we reproduce the result (18) (see Appendix G). The functions $\mathcal{F}_{1,2}(z)$ have the following asymptotics:

$$\mathcal{F}_1(z) = C_1^{(0)} z^2, \quad \mathcal{F}_2(z) = \mathcal{F}_2(0)[1 + C_2^{(0)} z^2], \quad |z| \ll 1, \tag{49}$$

and

$$\mathcal{F}_1(z) = C_1^{(\infty)} |z|^\gamma, \quad \mathcal{F}_2(z) = C_2^{(\infty)} |z|^{\gamma-1}, \quad |z| \gg 1, \tag{50}$$

where $C_{1,2}^{(0,\infty)}$ are numerical coefficients which satisfy the following relations:

$$C_1^{(0)} = \frac{2}{\pi}\int_0^\infty \frac{dx}{x}\mathcal{F}_2'(x), \quad C_1^{(\infty)} = C_2^{(\infty)}\Phi_\gamma. \tag{51}$$

We note that the numerical coefficients introduced above for the asymptotic expressions of the exact polarization operator and the self-energy can be found within $1/d_c$ expansion for 2D membrane embedded into $d_c + 2$-dimensional space [9]. We present the results of such calculations in Appendix H.

So far we analyze the exact self-energy in the universal regime (regions I_a and I_b in Fig. 2). The behavior of the self-energy beyond the universal regime is controlled by the lowest-order diagrams and discussed in Appendix I.

D. Attenuation of flexural phonons

The above results proves the form (18) of the exact Green's function and provides asymtotic expressions for the functions $\mathcal{F}_{1,2}$. The exact Green's function in the form of (18) implies that the spectrum of flexural phonons at $k \ll q_*$ is given as $\omega = s\omega_k$ where a complex number s solves the following equation:

$$s^2 - 1 + \mathcal{F}_1(s) + is\mathcal{F}_2(s) = 0. \tag{52}$$

The solution of this equation is a complex number s with, generically, $|s| \sim 1$. It implies that the imaginary part of the flexural phonon's spectrum $\mathrm{Im}s\,\omega_k$ is of the same order as its real part, $\mathrm{Re}s\,\omega_k$. In particular, if one defines the decay rate $1/\tau_k = \mathrm{Im}\Sigma^R_{\boldsymbol{k}}(\omega_k)/(\rho\omega_k)$, then one finds $\omega_k\tau_k \sim 1$. This poses several questions: (i) Why do we not see implications of such a short decay time in the theory of anomalous elasticity? and (ii) How can such strong decay of flexural phonons be observed? We will discuss both questions in the next sections.

V. ABSENCE OF IMPLICATION FOR THE CRUMPLING TRANSITION

The equilibrium stretching of membrane is determined by the condition that average displacement, cf. Eq. (6), vanishes in the absence of external tension

$$\langle\varepsilon_\alpha\rangle = \xi^2 - 1 + \sum_{\omega,\boldsymbol{k}} k_\alpha^2 \langle|h_{\boldsymbol{k},\omega}|^2\rangle = 0. \tag{53}$$

This equation determines dependence of the stretching factor ξ^2 on temperature as

$$\xi^2 = 1 - \tfrac{1}{2}\langle[\nabla h(\boldsymbol{x},t)]^2\rangle. \tag{54}$$

The temperature T_c, at which ξ^2 vanishes, determines the crumpling transition of a membrane from the flat to crumpled phase. Computing $\langle h^2(\boldsymbol{x},t)\rangle$, we find

$$\begin{aligned}\langle[\nabla h(\boldsymbol{x},t)]^2\rangle &= \int\frac{d\omega}{\pi}\int\frac{d^2\boldsymbol{k}}{(2\pi)^2}k^2\mathrm{Im}\mathcal{G}^R_{\boldsymbol{k}}(\omega)\coth\frac{\omega}{2T}\\ &\simeq 2T\int\frac{d^2\boldsymbol{k}}{(2\pi)^2}k^2\int\frac{d\omega}{\pi}\frac{\mathrm{Im}\mathcal{G}^R_{\boldsymbol{k}}(\omega)}{\omega}\\ &= 2T\int\frac{d^2\boldsymbol{k}}{(2\pi)^2}k^2\mathrm{Re}\mathcal{G}^R_{\boldsymbol{k}}(0)\\ &= \int\frac{d^2\boldsymbol{k}}{(2\pi)^2}\frac{2Tk^2}{\varkappa k^{4-\eta}q_*^{\eta}}.\end{aligned}\tag{55}$$

It is exactly the same result as in the static theory. Therefore, the attenuation of flexural phonons does not affect the crumpling transition. Similarly, one can demonstrate that all the other static effects known as anomalous elasticity are not affected by the phonon dynamics.

VI. TIME-DEPENDENT PAIR CORRELATION FUNCTION OF OUT-OF-PLANE DISPLACEMENT

In this section we discuss the time-dependent pair correlation function of the out-of-plane displacement $h(\boldsymbol{x},t)$. We start from the variance, $\langle h^2(\boldsymbol{x},t)\rangle$. As it follows from Eq. (55), $\langle h^2(\boldsymbol{x},t)\rangle$ diverges in the infrared such that

$$\langle h^2(\boldsymbol{x},t)\rangle \propto TL^{2\zeta}q_*^{-\eta}/\varkappa.\tag{56}$$

Here $L\gg 1/q_*$ denotes the membrane's system size. The roughness exponent equals [28]

$$\zeta = 1-\eta/2.\tag{57}$$

Next we consider a different time pair correlation function,

$$\begin{aligned}\langle[h(\boldsymbol{x},t)-h(\boldsymbol{x},0)]^2\rangle = 2\int\frac{d\omega}{\pi}\int\frac{d^2\boldsymbol{k}}{(2\pi)^2}\sin^2\frac{\omega t}{2}\coth\frac{\omega}{2T}\\ \times\,\mathrm{Im}\mathcal{G}^R_{\boldsymbol{k}}(\omega).\end{aligned}\tag{58}$$

Here the integrals are convergent both in ultraviolet and infrared. So we consider infinite membrane. Then integral over k is dominated by $k\sim[\rho\omega^2/(\varkappa q_*^{\eta})]^{1/(4-\eta)}$, which corresponds to the mass-shell condition $\omega_k=\omega$. Therefore, we find

$$\begin{aligned}\left\langle[h(\boldsymbol{x},t)-h(\boldsymbol{x},0)]^2\right\rangle \simeq 2W_\eta\frac{T}{\rho}\left(\frac{\rho}{\varkappa q_*^{\eta}}\right)^{\frac{2}{4-\eta}}\int_0^\infty\frac{d\omega}{\pi\omega}\\ \times\,\omega^{-\frac{4-2\eta}{4-\eta}}\sin^2\frac{\omega t}{2},\end{aligned}\tag{59}$$

where the constant

$$W_\eta=\int_0^\infty\frac{dx\,x^{(3-\eta/2)}\mathcal{F}_2(x^{-2+\eta/2})/\pi}{\{1-x^2[1-\mathcal{F}_1(x^{-2+\eta/2})]\}^2+x^{4-\eta}\mathcal{F}_2^2(x^{-2+\eta/2})}.\tag{60}$$

Integral over frequency is dominated by $\omega\sim 1/t$ such that we find

$$\left\langle[h(\boldsymbol{x},t)-h(\boldsymbol{x},0)]^2\right\rangle \simeq \widetilde{W}_\eta\frac{T}{\varkappa q_*^2}[\omega_* t]^{2\zeta/\mathsf{z}},\tag{61}$$

where $\widetilde{W}_\eta=-2^{2\zeta/z}\cos(\pi\zeta/z)\Gamma(-2\zeta/z)W_\eta/\pi$. We note the exact relation between dynamical and roughness exponents,

$$\mathsf{z}=1+\zeta=2-\eta/2.\tag{62}$$

The result (61) is valid for long times $\omega_* t\gg 1$. Since the exponent $2\zeta/\mathsf{z}=(2-\eta)/(2-\eta/2)<1$, Eq. (61) implies a subdiffusive dynamics of out-of-plane deformations.

One can combine Eqs. (56) and (61) in the following form:

$$\left\langle[h(\boldsymbol{x},t)-h(\boldsymbol{x},0)]^2\right\rangle = \frac{T}{\varkappa}L^{2\zeta}q_*^{-\eta}\,\Xi[\omega_* t/(q_*L)^{\mathsf{z}}],\tag{63}$$

where the scaling function $\Xi(y)$ has the following asymptotic behavior:

$$\Xi(y)\propto\begin{cases}\text{const}, & y\to 0,\\ y^{2\zeta/\mathsf{z}}, & y\to\infty.\end{cases}\tag{64}$$

For shorter times, $T^{-1}\ll t\ll\omega_*^{-1}$, the integral over the momentum in Eq. (58) is still dominated by the mass-shell condition. Since there is no renormalization of the bending rigidity for $k\gg q_*$, we find diffusive-type dynamics at $T^{-1}\ll t\ll\omega_*^{-1}$,

$$\langle[h(\boldsymbol{x},t)-h(\boldsymbol{x},0)]^2\rangle\sim\frac{T}{\varkappa q_*^2}\omega_* t.\tag{65}$$

We discuss significance of the above results in the next section.

VII. DISCUSSION AND CONCLUSION

A. Comparison with the generalized Langevin approach

One could try to describe the low-frequency dynamics of the 2D membrane phenomenologically by means of the Langevin-type approach. The form (18) of the exact Green's function for the out-of-plane displacement h at low frequencies suggests the following Langevin-type equation:

$$-\rho\tilde{D}k^2(q_*/k)^{\eta/2}\partial_t h_{\boldsymbol{k}}(t)=\rho\omega_{\boldsymbol{k}}^2h_{\boldsymbol{k}}(t)+k(q_*/k)^{\eta/4}f_{\boldsymbol{k}}(t).\tag{66}$$

Here $\tilde{D}=\mathcal{F}_2(0)D$ and a white-noise random force has the correlation function dictated by the fluctuation-dissipation relation,

$$\langle f(\boldsymbol{x},t)f(\boldsymbol{x}',t')\rangle=4T\tilde{D}\rho\delta(t-t')\delta(\boldsymbol{x}-\boldsymbol{x}').\tag{67}$$

We note that in contrast with Langevin-type equation used in Refs. [43–46], all terms of Eq. (66) contains explicit k dependence. We emphasize that Eq. (66) can be only used for study of long-time dynamics, $\omega_{\boldsymbol{k}}t\gg 1$, where $\omega_{\boldsymbol{k}}$ is fixed by the magnitude of a relevant wave vector, $k\sim 1/L$. In general, one could try to derive the Langevin-type equation for the considered problem with the help of Wyld technique (see Ref. [42] for details) or, alternatively, by means of the Keldysh path integral. We leave it for future works.

Another complication with application of a Langevin-type equation to the description of dynamics of a 2D membrane is nonlinearity (interaction of flexural phonos) which leads not only to renormalization of the bending rigidity and attenuation but also to real mode coupling [55,56]. The latter appears as nonlinear terms in the Langevin-type equation.

B. Attenuation of flexural phonons for membranes of higher dimensions

The Wyld technique has recently been used for analysis of classical dynamics (in the sense of inequality $\omega \ll T$) of a $D = 4 - \epsilon$-dimensional crystalline membrane [42]. Analyzing the perturbative renormalization group controlled by a small parameter $\epsilon \ll 1$, the authors of Ref. [42] essentially arrived at the same scaling form of the Green's function, cf. Eq. (18), and the same expression for the dynamical exponent z, cf. Eq. (57). Together with our result, this suggests that the scaling form (18) and Eq. (57) for z are valid for a membrane of arbitrary dimension $D \geqslant 2$.

C. Attenuation of in-plane phonons

Due to the $O(2)$ rotational symmetry existing for a membrane in the flat phase [10], the renormalization of in-plane phonons is intimately related with that of flexural phonons, cf. Eq. (13). In order to find the spectrum of in-plane phonons at low momentum, we use the relation $\omega \sim k(Y/\rho)^{1/2}$ in which Y is substituted by $1/\Pi_k^R(\omega)$. We note that we do not distinguish between longitudinal and transverse in-plane phonons. Since, as we will check below, the frequency of in-plane phonons is parametrically higher than that of flexural phonons, one needs to employ large-frequency asymptote of the polarization operator, Eq. (46). Then we find that the spectrum of the longitudinal and transverse in-plane phonons (at $k \ll q_*\sqrt{T/\varkappa}$) is given as

$$\omega_k^{(l,t)} = s_{l,t}\omega_*\left(\frac{k\sqrt{\varkappa}}{q_*\sqrt{T}}\right)^{\mathsf{z}'}, \quad \mathsf{z}' = \frac{(2-\eta/2)}{(1+\eta/2)}. \tag{68}$$

Here $s_{l,t}$ are some complex numbers. We note that the region of validity of Eq. (68) is determined by the inequality $Y\Pi_k^R(\omega_k^{(l,t)}) \gg 1$. Also we note that the assumption $\omega_k^{(l,t)} \gg \omega_k$ is satisfied indeed. At $k \gg q_*\sqrt{T/\varkappa}$ the spectrum of the in-plane phonons is not renormalized, $\omega_k^{(l,t)} \sim k$. Since at such momenta, $\omega_k^{(l,t)} \sim k\sqrt{Y/\rho} \gg \omega_*$, we use the following estimate in this region: $Y\mathrm{Im}\Pi_k^R(\omega_k^{(l,t)}) \sim q_*\sqrt{T}/(k\sqrt{\varkappa}) \ll 1$. Thus, attenuation becomes

$$\frac{1}{\tau_{\boldsymbol{k}}} \simeq \frac{\rho\left(\omega_{\boldsymbol{k}}^{(l,t)}\right)^2}{\rho\omega_{\boldsymbol{k}}^{(l,t)}}\left(\frac{q_*\sqrt{T}}{k\sqrt{\varkappa}}\right) \simeq \omega_*. \tag{69}$$

We emphasize that in contrast with the case of flexural phonons, the scaling of frequency with momentum in Eq. (68) is different from that one could envision on the basis of static renormalization of elastic moduli (13).

We expect validity of the result (68) for the dynamical exponent of the in-plane phonons for membranes of an arbitrary dimension $D \geqslant 2$. For $D = 4 - \epsilon$ our prediction contradicts to the result of Ref. [42]. We believe that the origin for such a discrepancy is that the static renormalization of elastic moduli (13) was used in Ref. [42] to derive the spectrum of in-plane phonons.

D. Flexural phonon attenuation beyond the universal regime

In the above discussion we consider the universal region of small frequency and momenta, $k \ll q_*$ and $\omega \ll \omega_*$. Although, such a situation realizes typically in experiments, it is worthwhile to discuss the behavior of the imaginary part of the self-energy at large wave vectors, $q_* \ll k \ll q_T = q_*/\sqrt{g}$ and frequencies, $\omega_* \ll |\omega| \ll T$ (regions II and III in Fig. 2). The estimates given in Appendix I result in the following behavior:

$$\mathrm{Im}\Sigma_{\boldsymbol{k}}^R(\omega) \sim \frac{T^2Y^2}{\varkappa^3}\begin{cases} \frac{Dk^{2+\eta}}{\omega q_*^{\eta}}, & \mathrm{II_a}: \ \omega \gg \omega_* \gg Dk^2, \\ \frac{Dk^2}{\omega}, & \mathrm{III_a}: \ \omega \gg Dk^2 \gg \omega_*, \\ \frac{\omega}{Dk^2}, & \mathrm{II_b \text{ and } III_b}: \ \omega \ll Dk^2, \ q_* \ll k. \end{cases} \tag{70}$$

Interestingly, near the mass shell, the imaginary part of the self-energy is enhanced by a factor $k/q_* \gg 1$ (see Fig. 2),

$$\mathrm{Im}\Sigma_{\boldsymbol{k}}^R(\omega) \sim \frac{T^2Y^2}{\varkappa^3}\frac{k}{q_*}, \quad |\omega - Dk^2| \ll \omega_*. \tag{71}$$

Estimating the attenuation coefficient of the flexural phonon with the momentum $q_* \ll k \ll q_T$ as $1/\tau_k = \mathrm{Im}\Sigma_{\boldsymbol{k}}^R(\omega_k^{(0)})/(\rho\omega_k^{(0)})$, we find that $\omega_k^{(0)}\tau_k \sim (k/q_*)^3 \gg 1$. Therefore, there is almost no attenuation of the spectrum of flexural phonons with high momenta $q_* \ll k \ll q_T$.

E. Benchmarking against experiments

In this paper we present detailed microscopic theory of phonon attenuation in two-dimensional flexible materials. We mention that the phonon spectrum in graphene has recently been measured by the method of the high-resolution electron energy loss spectroscopy [47]. We note that experimental data demonstrate some broadening of phonon spectrum. However, in order to perform detailed benchmarking of our theory, more detailed experimental data of the spectrum around the Γ point is needed.

F. Implications for mechanical nanoresonators

It is instructive to estimate numerical magnitudes of important parameters in our theory. Having in mind graphene as an example of two-dimensional crystalline membrane, we find that the Ginzburg length is $1/q_* \approx 1$ nm and $\omega_* \approx 200$ GHz. For $L \gg 1/q_*$, the frequency of typical out-of-plane deformation can be estimated as $\omega_{k\sim 1/L} \approx 3$ MHz for a typical size $L = 1$ μm. Also, Eq. (56) allows us to estimate typical amplitude of the flexural deformations as $h \sim 10$ nm for the same $L = 1$ μm.

Recently, the measurement of time-dependent out-of-plane fluctuations in graphene has been performed by means of scanning tunneling spectroscopy [52]. In agreement with our theory, the long-time dynamics characterized by the pair correlation function $\langle[h(\boldsymbol{x},t) - h(\boldsymbol{x},0)]^2\rangle$ was found to be subdiffusive. However, the corresponding exponent was estimated to be equal 0.3 in contrast to our prediction $2\zeta/\mathsf{z} \simeq 0.75$. Several possible reasons for such a discrepancy might be proposed. At first, the data in the experiment of Ref. [52] contain two types of fluctuations: fast small-amplitude fluctuations and slow large-amplitude excursions. While the former can be assumed to be the thermal fluctuations studied in our paper, the latter were related with spontaneous changing of local curvature. Such local buckling is not taken into account in our theory. Second, the scanning tunneling microscopy tip can induce a local tension that affects the dynamics of

thermal fluctuations. Third, the experimental data presented in Ref. [52] were collected from multiple graphene membranes. It is known [26] that a quenched random curvature is important for graphene samples. Different graphene flakes in the experiment of Ref. [52] could have a different realization of a quenched random curvature (due to some disorder). Therefore, one needs to study the dynamics of flexural phonons in the presence of disorder. We leave more detailed investigation of the effects discussed above for future work.

G. The effect of a nonzero tension

The theory presented in this work was developed for free-standing materials in the absence of tension, $\sigma \equiv 0$. However, if membrane is lying on a substrate with a hole, then the substrate imposes a stress on a part of the membrane above the hole. Therefore, the membrane experiences a nonzero tension σ.

As in the well-known Refs. [7,10,57], small tension, $\sigma \ll \sigma_* = \varkappa q_*^2$, (i) suppresses the renormalization of the bending rigidity at wave vectors $k < q_\sigma$, where $q_\sigma = q_*(\sigma/\sigma_*)^{1/(2-\eta)}$ and (ii) transforms the spectrum of flexural phonons into a soundlike one, $\omega_k^{(\sigma)} = k\sqrt{\sigma/\rho}$. Therefore, there is no surprise that tension affects the attenuation of flexural phonons. In particular, one can derive the following estimate [58]:

$$\mathrm{Im}\,\Sigma_{\boldsymbol{k}}^R\left[\omega_k^{(\sigma)}\right] \sim \varkappa_\sigma k^4, \qquad k \ll q_\sigma, \tag{72}$$

where $\varkappa_\sigma = \varkappa(q_*/q_\sigma)^\eta$. Therefore, the decay rate of the flexural phonon at $k \ll q_\sigma$ becomes

$$1/\tau_k^{(\sigma)} = \mathrm{Im}\,\Sigma_{\boldsymbol{k}}^R\left[\omega_k^{(\sigma)}\right]/\left[\rho\omega_k^{(\sigma)}\right] \sim (k/q_\sigma)^2\omega_k^{(\sigma)} \ll \omega_k^{(\sigma)}. \tag{73}$$

Therefore, a nonzero tension results in parametric narrowing of the spectral line for the flexural phonon. Interestingly, the width of spectral line becomes temperature dependent in the presence of a nonzero tension, $1/\tau_k^{(\sigma)} \sim T^\alpha$, where $\alpha = \eta/(2-\eta) \simeq 0.67$ [58].

Finally, we note that there are other mechanisms for decay of the out-of-plane displacement dynamics in nanoelectromechanical resonators [59]. Their discussion is beyond the scope of the present work.

H. Summary

To summarize we studied the attenuation of the phonons in free-standing 2D crystalline membranes. We explored high-temperature regime (relevant for experiments) in which flexural phonons can be treated classically, $T \gg \omega_k$. We found that in the universal regime, $k \ll q_*$, the broadening of the flexural phonon spectral line is of the order of the spectrum itself while at $q_* \ll k \ll q_T$ the broadening is parametrically suppressed (see Fig. 8). Focusing on the universal regime, we established the exact expression for the dynamical exponents z, see Eq. (62), and z', see Eq. (68), for flexural and in-plane phonons, respectively. We applied our theory to computation of the time-dependent pair correlation function of membrane's height and found its subdiffusive behavior at long times in qualitative accordance with the experiments. Finally, we discussed some future research directions.

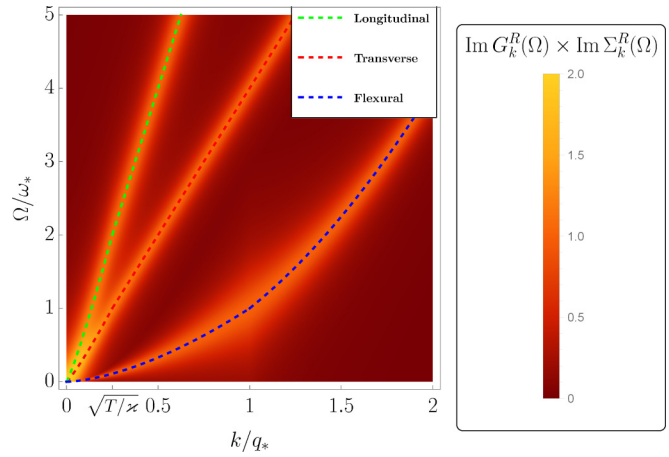

FIG. 8. Sketch of the dependence of the phonon spectral function on the momentum and frequency. For convenient normalization, we plot $\mathrm{Im}\mathcal{G}_{\boldsymbol{k}}^R(\omega)\mathrm{Im}\,\Sigma_{\boldsymbol{k}}^R(\omega)$ [Eqs. (18) and (68)]. We emphasize that change of the spectrum of flexural phonons occurs at $k \sim q_*$ while for the in-plane phonons it happens at $k \sim q_*\sqrt{T/\varkappa}$.

ACKNOWLEDGMENTS

The authors thank V. Kachorovskii for continuous interest in this work and for useful comments. The authors are grateful to E. Kats and V. Lebedev for fruitful discussions. The work was funded in part by the Russian Ministry of Science and Higher Educations and by the Basic Research Program of HSE.

APPENDIX A: THE EFFECT OF DYNAMICAL PART OF INTERACTION BETWEEN FLEXURAL PHONONS MEDIATED BY IN-PLANE ONES

In this Appendix we present an estimate for contribution of dynamical part of bare interaction between flexural phonons to $\mathrm{Im}\,\Sigma_{\boldsymbol{k}}^R(\omega)$.

The self-energy correction in the first order of perturbation theory is given by [see Ref. [25], Eq. (B6)]:

$$\mathrm{Im}\,\Sigma_{\boldsymbol{k}}^{(m),R}(\omega) = T\omega\int\frac{d\Omega}{2\pi}\int\frac{d^2\boldsymbol{q}}{(2\pi)^2}\frac{(\boldsymbol{k}\cdot\boldsymbol{q}-q^2)^2}{q^4}(\boldsymbol{q}\cdot\boldsymbol{k})^2 \times \frac{\mathrm{Im}R_{\boldsymbol{q}}^{(mmmm),R}(\Omega)}{\Omega}\frac{\mathrm{Im}G_{\boldsymbol{k}+\boldsymbol{q}}^R(\Omega+\omega)}{\omega+\Omega}, \tag{A1}$$

where

$$R_{\boldsymbol{q}}^{(mmmm)}(i\Omega) = \rho\frac{(2\mu+\lambda)\Omega^2}{(2\mu+\lambda)q^2+\rho\Omega^2}. \tag{A2}$$

This is one of the four additional interaction terms, but all of them have the same scaling properties. For conciseness, we will only evaluate this term.

As in the main text, we focus on the region $k \ll q_*$. In this domain, $\omega_{\boldsymbol{k}} = Dk^2 \ll c_l k = \varepsilon_{\boldsymbol{k}}$, where $c_l = \sqrt{(2\mu+\lambda)/\rho}$ denotes the speed of longitudinal sound mode. We are mostly interested in $\omega \sim \omega_{\boldsymbol{k}}$, since the decay rate is determined by the frequency on the mass shell. First, we find the imaginary part

of the retarded interaction:

$$\mathrm{Im}R_{\boldsymbol{q}}^{(mmmm),R}(\Omega)=\frac{\pi(2\mu+\lambda)\Omega}{2}\sum_{s=\pm}\delta(\Omega+s\varepsilon_{\boldsymbol{q}}). \tag{A3}$$

The imaginary part of the retarded Green's function becomes

$$\mathrm{Im}G_{\boldsymbol{q}}^{R}(\omega)=\frac{\pi}{2\rho\omega}\sum_{s=\pm}\delta(\omega+s\omega_{\boldsymbol{q}}). \tag{A4}$$

We then substitute Eqs. (A3) and (A4) into Eq. (A1) and integrate over Ω,

$$\begin{aligned}\mathrm{Im}\Sigma_{\boldsymbol{k}}^{(m),R}(\omega)=&\frac{c_l^2T\omega}{32\pi}\int d^2\boldsymbol{q}\frac{(\boldsymbol{k}\cdot\boldsymbol{q}-q^2)^2}{q^4}\frac{(\boldsymbol{q}\cdot\boldsymbol{k})^2}{\omega_{\boldsymbol{k}+\boldsymbol{q}}^2}\\&\times\sum_{s=\pm}[\delta(s\varepsilon_{\boldsymbol{q}}+\omega+\omega_{\boldsymbol{k}+\boldsymbol{q}})\\&+\delta(s\varepsilon_{\boldsymbol{q}}+\omega-\omega_{\boldsymbol{k}+\boldsymbol{q}})].\end{aligned} \tag{A5}$$

We proceed by introducing new variables $\boldsymbol{k}=k\boldsymbol{n}$, $\boldsymbol{q}=k\boldsymbol{r}$, $z=\omega/\omega_{\boldsymbol{k}}$ and by making the expressions dimensionless. We also introduce the parameter $\alpha_k=\varepsilon_{\boldsymbol{k}}/\omega_{\boldsymbol{k}}\gg 1$. In terms of those variables, we obtain

$$\begin{aligned}\mathrm{Im}\Sigma_{\boldsymbol{k}}^{(m),R}(\omega)=&\frac{T}{\varkappa}\frac{\rho\omega_{\boldsymbol{k}}\omega}{32\pi}\int d^2\boldsymbol{r}\frac{[(\boldsymbol{r}\cdot\boldsymbol{n})-r^2]^2}{r^4}\frac{\alpha_k^2(\boldsymbol{r}\cdot\boldsymbol{n})^2}{|\boldsymbol{r}+\boldsymbol{n}|^4}\\&\times\sum_{s=\pm1}[\delta(s\alpha_k r+z+|\boldsymbol{r}+\boldsymbol{n}|^2)\\&+\delta(s\alpha_k r+z-|\boldsymbol{r}+\boldsymbol{n}|^2)].\end{aligned} \tag{A6}$$

At large α_k and $z\sim 1$, the argument of δ function is zero either at $r\sim\alpha_k\gg 1$ or $r\sim 1/\alpha_k\ll 1$. In both cases, we can approximate $|\boldsymbol{r}+\boldsymbol{n}|^2\sim r^2+1$.

Then the integral over the angle can be evaluated separately:

$$\int_0^{2\pi}d\varphi\frac{(\boldsymbol{r}\cdot\boldsymbol{n}-r^2)^2}{r^4}\frac{(\boldsymbol{r}\cdot\boldsymbol{n})^2}{|\boldsymbol{r}+\boldsymbol{n}|^4}\simeq\begin{cases}\frac{3\pi}{4}, & r\ll 1,\\ \frac{\pi}{r^2}, & r\gg 1.\end{cases} \tag{A7}$$

We then integrate over r using asymptotics (A7) and obtain for $z>0$:

$$\mathrm{Im}\Sigma_{\boldsymbol{k}}^{(m),R}(\omega)=\frac{T}{32\varkappa}\rho\omega_{\boldsymbol{k}}\omega\left[2+\frac{3}{4}(|z-1|+z+1)\right]. \tag{A8}$$

We can see that the correction is small in virtue of the small parameter $T/\varkappa\ll 1$. The same parameter controls other corrections occurring from dynamics of the in-plane phonons.

APPENDIX B: EVALUATION OF THE STATIC LIMIT OF THE DIAGRAM IN FIG. 4

In this Appendix we demonstrate how the static limit of the diagram shown in Fig. 4 transforms into Eq. (26) at high temperatures. The aforementioned diagram is given by

$$\begin{aligned}\Sigma_{\boldsymbol{k}}^{(2)}(0)=-4\sum_{\boldsymbol{q},\boldsymbol{Q},\Omega,\omega}&S(\boldsymbol{q},\boldsymbol{Q})G_{\boldsymbol{k}+\boldsymbol{q}}(i\omega)G_{\boldsymbol{k}+\boldsymbol{Q}}(i\Omega)\\&\times G_{\boldsymbol{k}+\boldsymbol{q}+\boldsymbol{Q}}(i\omega+i\Omega)N_{\boldsymbol{q}}(i\omega)N_{\boldsymbol{Q}}(i\Omega),\end{aligned} \tag{B1}$$

where for convenience we introduced

$$S(\boldsymbol{q},\boldsymbol{Q})=\frac{[(\boldsymbol{k}+\boldsymbol{Q})\times\boldsymbol{q}]^2}{q^2}\frac{[(\boldsymbol{k}+\boldsymbol{q})\times\boldsymbol{Q}]^2}{Q^2}\frac{[\boldsymbol{k}\times\boldsymbol{q}]^2}{q^2}\frac{[\boldsymbol{k}\times\boldsymbol{Q}]^2}{Q^2}. \tag{B2}$$

At first, we transform the sum over bosonic Matsubara frequencies ω into the integral along the real axis

$$\begin{aligned}\Sigma_{\boldsymbol{k}}^{(2)}(0)=-4\sum_{\boldsymbol{q},\boldsymbol{Q},\Omega}&S(\boldsymbol{q},\boldsymbol{Q})N_{\boldsymbol{Q}}(i\Omega)G_{\boldsymbol{k}+\boldsymbol{Q}}(i\Omega)\int\frac{d\omega}{2\pi}\\&\times\coth\left(\frac{\omega}{2T}\right)\{G_{\boldsymbol{k}+\boldsymbol{q}+\boldsymbol{Q}}(\omega+i\Omega)\\&\times\mathrm{Im}[N_{\boldsymbol{q}}^R(\omega)G_{\boldsymbol{k}+\boldsymbol{q}}^R(\omega)]\\&+N_{\boldsymbol{q}}(\omega-i\Omega)G_{\boldsymbol{k}+\boldsymbol{q}}(\omega-i\Omega)\mathrm{Im}G_{\boldsymbol{k}+\boldsymbol{q}+\boldsymbol{Q}}^R(\omega)\}.\end{aligned} \tag{B3}$$

Next, similarly, we transform the sum over bosonic Matsubara frequencies Ω into the integral over real axis,

$$\begin{aligned}\Sigma_{\boldsymbol{k}}^{(2)}(0)=-4\sum_{\boldsymbol{q},\boldsymbol{Q}}&S(\boldsymbol{q},\boldsymbol{Q})\int\frac{d\Omega d\omega}{(2\pi)^2}\coth\left(\frac{\Omega}{2T}\right)\coth\left(\frac{\omega}{2T}\right)\\&\times\{\mathrm{Im}[N_{\boldsymbol{Q}}^R(\Omega)G_{\boldsymbol{k}+\boldsymbol{Q}}^R(\Omega)G_{\boldsymbol{k}+\boldsymbol{q}+\boldsymbol{Q}}^R(\omega+\Omega)]\\&\times\mathrm{Im}[N_{\boldsymbol{q}}^R(\omega)G_{\boldsymbol{k}+\boldsymbol{q}}^R(\omega)]+\mathrm{Im}G_{\boldsymbol{k}+\boldsymbol{q}+\boldsymbol{Q}}^R(\omega)\\&\times\mathrm{Im}[N_{\boldsymbol{Q}}^R(\Omega)G_{\boldsymbol{k}+\boldsymbol{Q}}^R(\Omega)N_{\boldsymbol{q}}^A(\omega-\Omega)G_{\boldsymbol{k}+\boldsymbol{q}}^A(\omega-\Omega)]\}.\end{aligned} \tag{B4}$$

In the high-temperature regime ($T\gg|\Omega|,|\omega|$) the hyperbolic cotangent can be replaced by the first term in its Taylor series. Then, using Kramers-Kronig relations, we perform integrals over ω and Ω, and, thus, we derive (26).

APPENDIX C: FORMULATION OF DYNAMICAL PERTURBATION THEORY

In this Appendix we demonstrate how the perturbation theory around the Green's function (27) can be formulated in a regular fashion.

The "bare" Green's function is related to the Green's function defined in Eq. (27) by the Dyson equation with static self-energy,

$$G_{\boldsymbol{k}}(i\omega)=\left[\mathcal{G}_{\boldsymbol{k}}^{-1}(i\omega)+\Sigma_{\boldsymbol{k}}(0)\right]^{-1}. \tag{C1}$$

We can also rewrite this equation in terms of the infinite series

$$G_{\boldsymbol{k}}(i\omega)=\mathcal{G}_{\boldsymbol{k}}(i\omega)-\mathcal{G}_{\boldsymbol{k}}(i\omega)\Sigma_{\boldsymbol{k}}(0)\mathcal{G}_{\boldsymbol{k}}(i\omega)+\ldots. \tag{C2}$$

To compute the dynamical self-energy corrections, we need to insert the series from Eq. (C2) into the series for $\Sigma_{\boldsymbol{k}}(i\omega)-\Sigma_{\boldsymbol{k}}(0)$ (see Fig. 9). Calculation of the imaginary part, $\mathrm{Im}[\Sigma_{\boldsymbol{k}}^R(\omega)-\Sigma_{\boldsymbol{k}}^R(0)]$, is more convenient because $\mathrm{Im}\Sigma_{\boldsymbol{k}}^R(0)=0$.

The first term in the right-hand side of Eq. (C2) forms a sequence of self-energy diagrams, where all the "bare" Green's functions are substituted by the one from Eq. (27). These contributions are termed as the main terms. The next terms in the right-hand side of Eq. (C2) produce additional set of diagrams (extra terms).

The above statements can be illustrated by diagrams in Fig. 9. In Fig. 9(a), the diagram of the first order in dynam-

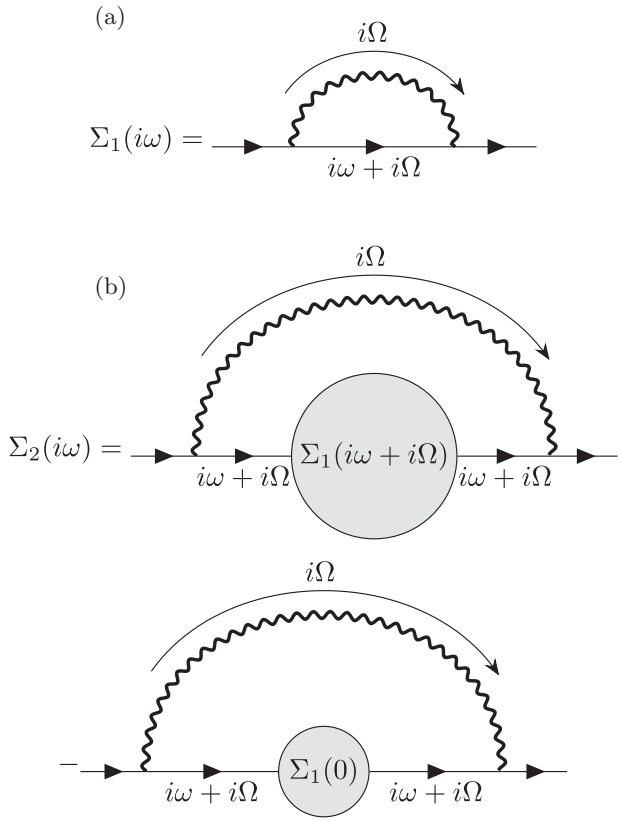

FIG. 9. (Top) First-order of interaction self-energy correction, (middle) second-order main term, and (bottom) second-order extra term. Wiggly lines denote screened interaction (20), and solid lines denote Green's functions (27).

ically screened interaction is shown. There is a solid line in the "bare" Green's function G. Substituting it with the second term in the right-hand side of (C2), we produce the second diagram in Fig. 9(b). We note that the extra diagram is formally of infinite order in dynamically screened interaction, since it involves the exact static self-energy. In the same way diagrams of the second order in the dynamically screened interaction produces extra diagrams with the exact static self-energy.

Now we argue that extra terms do not spoil the scaling of the main self-energy corrections in the universal regime $q \ll q_*$. Indeed, the static self-energy, $\Sigma_{\boldsymbol{k}}(0) = \varkappa k^{4-\eta} q_*^{\eta}$, has the same k dependence as the dynamical self-energy at the mass shell, $\omega = \omega_k$. Similarly to the main terms, the frequency integrals in extra terms are still dominated by the frequencies corresponding to the mass-shell conditions. Therefore, extra terms produce the same scaling between frequency and momentum as the main ones.

The same argument allows us to work with screened Green's functions (27) (instead of the "bare" ones) in the polarization operator (29).

APPENDIX D: COMPUTATION OF ASYMPTOTIC EXPRESSION FOR THE POLARIZATION OPERATOR (33)

In this Appendix we present a derivation of Eqs. (30) and (31). Using Eq. (A4) for the imaginary part of the retarded Green's function, we obtain from Eq. (29),

$$\mathrm{Im}\Pi^R_{\boldsymbol{q}}(\Omega) = \frac{\pi T\Omega}{12 q_*^{2\eta}} \int \frac{d^2\boldsymbol{k}}{(2\pi)^2} \frac{[\boldsymbol{k}\times\boldsymbol{q}]^4}{q^4} \frac{1}{\varkappa k^{4-\eta}} \frac{1}{\varkappa|\boldsymbol{k}+\boldsymbol{q}|^{4-\eta}} \times \sum_{s=\pm1} [\delta(s\Omega+\omega_k - \omega_{\boldsymbol{k}+\boldsymbol{q}}) + \delta(s\Omega+\omega_k+\omega_{\boldsymbol{k}+\boldsymbol{q}})]. \tag{D1}$$

In order to calculate this integral, it is convenient to introduce new variable $\boldsymbol{y} = |\boldsymbol{k}+\boldsymbol{q}|$. We note that the Jacobian of this transformation is

$$\left|\frac{\partial(k,\varphi)}{\partial(k,y)}\right| = \frac{2y}{kq\sin\varphi}. \tag{D2}$$

The factor of 2 emerges because the integrand is an even function of the angle, and our substitution is single valued only in one half-plane. In terms of new variables integral takes the form

$$\mathrm{Im}\,\Pi^R_{\boldsymbol{q}}(\Omega) = \frac{T}{24\pi} \frac{\Omega}{\varkappa^2 q_*^{2\eta} q} \int y dy dk \frac{k^{\eta}\sin^3\varphi}{y^{4-\eta}} \times \sum_{s=\pm} [\delta(s\Omega+\omega_{\boldsymbol{k}}-\omega_{\boldsymbol{y}}) + \delta(s\Omega+\omega_{\boldsymbol{k}}+\omega_{\boldsymbol{y}})]. \tag{D3}$$

We then proceed by making the integral dimensionless by introducing variables $z = \Omega/\omega_{\boldsymbol{q}}$, $x = k/q$, $a = y/q$. We also rewrite $\sin^3\varphi$ in terms of new variables. Then we obtain

$$\mathrm{Im}\,\Pi^R_{\boldsymbol{q}}(\Omega) = \frac{T}{24\pi} \frac{z}{\varkappa^2 q_*^{2\eta} q^{2-2\eta}} \int_0^{\infty} dx \int_{|x-1|}^{|x+1|} da \frac{x^{\eta}}{a^{3-\eta}} \sum_{s=\pm} \times [\delta(sz+x^{2-\eta/2} - a^{2-\eta/2}) + \delta(sz+x^{2-\eta/2}+a^{2-\eta/2})] \times \left[1 - \left(\frac{x}{2} + \frac{1}{2x} - \frac{a^2}{2x}\right)^2\right]^{3/2}. \tag{D4}$$

The integral in this form can be evaluated in different limits. For $z \to 0$, we find

$$\mathrm{Im}\,\Pi^R_{\boldsymbol{q}}(\Omega) = \frac{T}{24\pi} \frac{z}{\varkappa^2 q_*^{2\eta} q^{2-2\eta}} \int_0^{\infty} dx \int_{|x-1|}^{|x+1|} \frac{x^{\eta}}{a^{3-\eta}} \times \left[1 - \left(\frac{x}{2}+\frac{1}{2x} - \frac{a^2}{2x}\right)^2\right]^{3/2} \times [\delta(x^{2-\eta/2} - a^{2-\eta/2})]. \tag{D5}$$

This integral can be computed exactly. This way we obtain [$\mathcal{P}_2^{(0)}(z)$ is defined according to Eq. (33)]

$$\mathcal{P}_2^{(0)}(z) \simeq C_{\eta}^{(0)} z,$$
$$C_{\eta}^{(0)} = \frac{2^{2-3\eta/2}\Gamma^2(2-\eta/2)\Gamma(3/2+\eta/2)\Gamma(3/2-5\eta/4)}{(1-\eta/4)\Gamma(1+\eta/2)\Gamma(1-\eta)\Gamma(4-5\eta/4)}. \tag{D6}$$

In the opposite limit $z \gg 1$ the integral is somewhat more complicated. In this case we will return to the representation

of the integral in terms of the momentum and the angle

$$\mathrm{Im}\,\Pi^R_{\boldsymbol{q}}(\Omega) = \frac{T}{24\pi}\frac{z}{\varkappa^2 q_*^{2\eta} q^{2-2\eta}}\int_0^\infty dx x^{\eta+1}\int_0^\pi d\varphi \sin^4\varphi \times \frac{\delta[z - x^{2-\eta/2} - (x^2+1+2x\cos\varphi)^{1-\eta/4}]}{(x^2+1+2x\cos\varphi)^{2-\eta/2}}. \tag{D7}$$

The other delta functions were excluded because they give subdominant contributions to asymptotics. It can be seen that due to the δ function, integration over x sets $x^{2-\eta/2} \approx z/2$. Hence, we find

$$\mathrm{Im}\,\Pi^R_{\boldsymbol{q}}(\Omega) = \frac{T}{24\pi(4-\eta)}\frac{z}{\varkappa^2 q_*^{2\eta} q^{2-2\eta}} \times \int_0^\pi d\varphi \frac{(z/2)^{\frac{3\eta}{4-\eta}}}{(z/2)^2}\sin^4\varphi. \tag{D8}$$

Integrating over φ, we obtain

$$\mathcal{P}_2^{(0)}(z) \simeq C_\eta^{(\infty)} z^{-(1-\eta)/(1-\eta/4)},$$
$$C_\eta^{(\infty)} = \frac{2^{\eta+(1-\eta)/(1-\eta/4)}\sqrt{\pi}\Gamma^2(2-\eta/2)\Gamma(3/2+\eta/2)}{(4-\eta)\Gamma(1+\eta/2)\Gamma(1-\eta)}. \tag{D9}$$

In order to find the real part of the polarization operator, $\mathcal{P}_1^{(0)}(z)$, we will use the Kramers-Kronig relation,

$$\mathcal{P}_1^{(0)}(z) = 1 + \frac{2z^2}{\pi}\mathrm{p.v.}\int_0^\infty \frac{dy}{y}\frac{\mathcal{P}_2^{(0)}(y)}{y^2-z^2}. \tag{D10}$$

Let us introduce $p_2(y) = \mathcal{P}_2^{(0)}(y)/y$, then we find

$$\mathcal{P}_1^{(0)}(z) = 1 + \frac{z}{\pi}\int_0^\infty \frac{dy}{y}[p_2(y+z) - p_2(y-z)]. \tag{D11}$$

At $z \to 0$ we can expand the right-hand side of the above equation in z and find

$$\mathcal{P}_1^{(0)}(z) \simeq 1 + \frac{2z^2}{\pi}\int_0^\infty \frac{dy}{y}\left[p_2'(y) + \frac{z^2}{6}p_2'''(y)\right]. \tag{D12}$$

We note that for $\eta = 0$ the integral $\int_0^\infty dy\, p_2'(y)/y = 0$. For $\eta \neq 0$ it is nonzero, and

$$\mathcal{P}_1^{(0)}(z) \simeq 1 + \frac{2z^2}{\pi}\int_0^\infty \frac{dy}{y}\left[\mathcal{P}_2^{(0)}(y)/y\right]'. \tag{D13}$$

At $z \gg 1$ we shall use the following relation:

$$\mathcal{P}_1^{(0)}(z) = \int_0^\infty \frac{dy}{\pi y}\left[\mathcal{P}_2^{(0)}(y+z) + \mathcal{P}_2^{(0)}(y-z)\right] = \int_0^\infty \frac{dy}{\pi y}\mathcal{P}_2^{(0)}(y+z) - \int_0^z \frac{dy}{\pi y}\mathcal{P}_2^{(0)}(z-y) + \int_z^\infty \frac{dy}{\pi y}\mathcal{P}_2^{(0)}(y-z). \tag{D14}$$

Now we estimate the integrals using the asymptotic (D9) of $\mathcal{P}_2^{(0)}(y)$ at $y \gg 1$,

$$\int_0^\infty \frac{dy}{y}\mathcal{P}_2^{(0)}(y+z) \simeq C_\eta^{(\infty)}\int_\delta^\infty \frac{dy}{y(y+z)^\gamma} \simeq C_\eta^{(\infty)} z^{-\gamma}\left[\ln\frac{z}{\delta} - \gamma_E - \psi(\gamma)\right],$$
$$\int_\delta^z \frac{dy}{y}\mathcal{P}_2^{(0)}(z-y) \simeq C_\eta^{(\infty)}\int_\delta^z \frac{dy}{y(z-y)^\gamma} \simeq C_\eta^{(\infty)} z^{-\gamma}\left[\ln\frac{z}{\delta} - H(-\gamma)\right],$$
$$\int_z^\infty \frac{dy}{y}\mathcal{P}_2^{(0)}(y-z) \simeq C_\eta^{(\infty)}\int_z^\infty \frac{dy}{y(y-z)^\gamma} \simeq C_\eta^{(\infty)} z^{-\gamma}\frac{\pi}{\sin(\pi\gamma)}, \tag{D15}$$

where we note that $\gamma = (1-\eta)/(1-\eta/4) < 1$. Also $H(n) = \sum_{i=1}^n 1/i$ denotes the harmonic number. Therefore, we obtain at $z \gg 1$

$$\mathcal{P}_1^{(0)}(z) \propto z^{-\frac{1-\eta}{1-\eta/4}}. \tag{D16}$$

We note that due to the presence of $\ln z$ contributions in Eq. (D15) it is not possible to determine the exact prefactor in the asymptotic expression for $\mathcal{P}_1^{(0)}(z)$. Nevertheless, our approach guarantees to give us the correct power-law behavior of $\mathcal{P}_1^{(0)}(z)$ at $z \gg 1$.

APPENDIX E: COMPUTATION OF ASYMPTOTIC EXPRESSION FOR THE SELF-ENERGY (39)

In this Appendix we present derivation of asymptotic expressions for the functions $\mathcal{F}_1^{(1)}(z)$ and $\mathcal{F}_2^{(1)}(z)$. We use the approach similar to Appendix D. At first, we introduce new variables $z = \omega/\omega_{\boldsymbol{k}}$, $x = q/k$, $a = y/k$, where $y = |\boldsymbol{k}+\boldsymbol{q}|$. Then after integration over Ω in Eq. (28), we find

$$\mathrm{Im}\,\Sigma^{(1),R}_{\boldsymbol{k}}(\omega) = \frac{\rho\omega\omega_{\boldsymbol{k}}}{6A_\eta\pi^2}\int \frac{x^{2-2\eta}dxda\sin^3\varphi}{a^{3-\eta}} \times \sum_{s=\pm}\mathcal{X}^{(0)}\left(\frac{z+sa^{2-\eta/2}}{x^{2-\eta/2}}\right)\frac{1}{(z+sa^{2-\eta/2})}, \tag{E1}$$

where $\mathcal{X}^{(0)}(y) = \mathcal{P}_2^{(0)}(y)/[|\mathcal{P}_1^{(0)}(y)|^2 + |\mathcal{P}_2^{(0)}(y)|^2]$. Below we are not interested in numerical factors for reasons discussed in Appendix C. Therefore, prefactors from now on will be omitted.

The integral in the form of Eq. (E1) can be evaluated in different limits. For $z \ll 1$ we neglect z under the integral signs and obtain

$$\mathrm{Im}\,\Sigma^{(1),R}_{k}(\omega) = \frac{\rho\omega\omega_{\boldsymbol{k}}}{3A_\eta\pi^2}\int \frac{x^{2-2\eta}dxda\sin^3\varphi}{a^{5-3\eta/2}}\mathcal{X}_2^{(0)}\left[\left(\frac{a}{x}\right)^{2-\eta/2}\right]. \tag{E2}$$

This integral converges. Therefore, for small z the imaginary part of the self-energy behaves according to Eq. (40).

In order to analyze the limit $z \gg 1$, we neglect a in comparison with z wherever it is possible. Then we obtain

$$\mathrm{Im}\,\Sigma_k^{(1),R}(\omega) = \frac{\rho\omega\omega_{\boldsymbol{k}}}{3A_\eta\pi^2}\int_0^\infty dx\frac{x^{2-2\eta}}{z}\mathcal{X}^{(0)}\left(\frac{z}{x^{2-\eta/2}}\right) \times \int_{|x-1|}^{x+1}\frac{da}{a^{3-\eta}}\left[1-\left(\frac{a^2-1-x^2}{2x}\right)^2\right]^{3/2}. \tag{E3}$$

To obtain the asymptotics of the above expression, we evaluate the integral over a in two domains, $x \ll 1$ and $x \gg 1$,

$$\int_{|x-1|}^{x+1}\frac{da}{a^{3-\eta}}\left[1-\left(\frac{a^2-1-x^2}{2x}\right)^2\right]^{3/2} \approx \begin{cases}\frac{3\pi x}{8}, & x \ll 1,\\ \frac{3\pi}{8x^{3-\eta}}, & x \gg 1.\end{cases} \tag{E4}$$

Since we are only interested in the power dependence of the imaginary part of the self-energy on frequency, z, we will integrate the asymptotic expression (E4) within the limits of the applicability of the approximation. Thus, we neglect the difference of the function from its asymptotics in a parametrically small region where this function has no singularities. Then we find

$$\mathrm{Im}\,\Sigma_k^{(1),R}(\omega) = \frac{\rho\omega\omega_{\boldsymbol{k}}}{3A_\eta\pi^2}\left[\int_0^{\sim 1} dx\frac{x^{3-2\eta}}{z}\mathcal{X}^{(0)}\left(\frac{z}{x^{2-\eta/2}}\right) + \int_{\sim 1}^\infty dx\frac{1}{zx^{1+\eta}}\mathcal{X}^{(0)}\left(\frac{z}{x^{2-\eta/2}}\right)\right]. \tag{E5}$$

Next, we use asymptotics of the polarization operator, cf. Eqs. (35) and (38), to obtain

$$\mathrm{Im}\,\Sigma_k^{(1),R}(\omega) \sim \rho\omega\omega_{\boldsymbol{k}}\frac{z^\gamma}{z}\left[\int_0^{\sim 1} dx\,x + \int_{\sim 1}^\infty \frac{dx}{x^{3+\eta/2}}\right] \sim \rho\omega\omega_{\boldsymbol{k}}(\omega/\omega_k)^{\gamma-1}. \tag{E6}$$

In order to find the real part of the self-energy and to derive Eq. (43), one can employ the similar analysis as presented in Appendix D.

APPENDIX F: COMPUTATION OF ASYMPTOTICS FOR THE EXACT POLARIZATION OPERATOR (44)

In this Appendix we present arguments for the scaling form (44) of the exact polarization operator and compute its asymptotic expressions. Let us consider the polarization operator computed as a bubble of the two exact Green's function, cf. Eq. (29):

$$\mathrm{Im}\Pi_{\boldsymbol{q}}^{(b),R}(\Omega) = \frac{2T\Omega}{3}\int\frac{d\omega}{2\pi}\int\frac{d^2\boldsymbol{k}}{(2\pi)^2}\frac{[\boldsymbol{k}\times\boldsymbol{q}]^4}{q^4}\frac{\mathrm{Im}\mathcal{G}_{\boldsymbol{k}}^R(\omega)}{\omega} \times \frac{\mathrm{Im}\mathcal{G}_{\boldsymbol{k}+\boldsymbol{q}}^R(\omega+\Omega)}{\omega+\Omega}. \tag{F1}$$

For simplicity, we denote

$$\frac{\mathrm{Im}\mathcal{G}_{\boldsymbol{k}}^R(\omega)}{\omega} = \frac{1}{\rho\omega_{\boldsymbol{k}}^3}\mathcal{A}\left(\frac{\omega}{\omega_{\boldsymbol{k}}}\right), \tag{F2}$$

where

$$\mathcal{A}(z) = \frac{\mathcal{F}_2(z)}{[z^2+\mathcal{F}_1(z)-1]^2+z^2\mathcal{F}_2^2(z)}. \tag{F3}$$

In order to make the integral dimensionless, we introduce new variables: $\boldsymbol{y} = \boldsymbol{q}+\boldsymbol{k}$, $z = \Omega/\omega_{\boldsymbol{q}}$, $\tau = \omega/\omega_{\boldsymbol{q}}$, $k = xq$, $y = aq$, where $a = (1+x^2+2x\cos\varphi)^{1/2}$. In terms of new variables the integral can be rewritten as

$$\mathrm{Im}\Pi_{\boldsymbol{q}}^{(b),R} = \frac{2Tz}{3(2\pi)^3\varkappa^2q_*^{2\eta}q^{2-2\eta}}\int d\tau\int\frac{dxd\varphi\sin^4(\varphi)}{x^{1-3\eta/2}a^{6-3\eta/2}} \times \mathcal{A}\left(\frac{\tau}{x^{2-\eta/2}}\right)\mathcal{A}\left(\frac{z+\tau}{a^{2-\eta/2}}\right). \tag{F4}$$

First, we consider the case $z \to \infty$. In that limit we find

$$\mathrm{Im}\Pi_{\boldsymbol{q}}^{(b),R} = \frac{2Tz}{3(2\pi)^3\varkappa^2q_*^{2\eta}q^{2-2\eta}}\int\frac{dxd\varphi\sin^4(\varphi)x^{1+\eta}}{a^{6-3\eta/2}} \times \mathcal{A}^{(1)}\left(\frac{z}{a^{2-\eta/2}}\right)\int\frac{d\tau}{x^{2-\eta/2}}\mathcal{A}^{(1)}\left(\frac{\tau}{x^{2-\eta/2}}\right). \tag{F5}$$

The integral over τ converges and provides essentially a constant factor for the integral. Taking into account the fact that the integral is dominated by $a^{2-\eta/2} \ll z$ and $x \gg 1$, we substitute the asymptotic form of $\mathcal{A}(x)$,

$$\mathcal{A}(x) \sim x^{\gamma-5}, \quad x \gg 1. \tag{F6}$$

In the region $x \gg 1$ we can substitute a with x, thus separating integral over φ. Making these approximations, we find asymptotics of the imaginary part of the polarization operator as follows:

$$\mathrm{Im}\Pi_{\boldsymbol{q}}^{(b),R} \sim \frac{Tz}{\varkappa^2q_*^{2\eta}q^{2-2\eta}}\int_1^{z^{1/(2-\eta/2)}}\frac{dxx^{1+\eta}}{x^{6-3\eta/2}} \times \left(\frac{z}{x^{2-\eta/2}}\right)^{\gamma-5} \sim \frac{T}{\varkappa^2q_*^{2\eta}q^{2-2\eta}}z^{-\gamma}. \tag{F7}$$

In the limit of small frequencies, $z \to 0$, we find

$$\mathrm{Im}\Pi_{\boldsymbol{q}}^{(b),R} = \frac{2Tz}{3(2\pi)^3\varkappa^2q_*^{2\eta}q^{2-2\eta}}\int d\tau\int\frac{dxd\varphi\sin^4(\varphi)}{x^{1-3\eta/2}a^{6-3\eta/2}} \times \mathcal{A}^{(1)}\left(\frac{\tau}{x^{2-\eta/2}}\right)\mathcal{A}^{(1)}\left(\frac{\tau}{a^{2-\eta/2}}\right) \sim z. \tag{F8}$$

Therefore, using the exact Green's functions we reproduce exactly the same asymptotic expressions for the imaginary part of the polarization operator as we found in Appendix D. Furthemore, due to the Kramers-Kronig relations, the scaling of asymptotic expression for the real part of the polarization operator is also the same as given in Appendix D. We note that consideration of more complicated diagrams for the polarization operator does not change the scaling.

In order to draw any conclusions we also need to check whether self-energy behaves in the way consistent with the form of the exact Green's function. This will be done in Appendix G.

APPENDIX G: COMPUTATION OF ASYMPTOTICS FOR EXACT SELF-ENERGY (15)

In this Appendix we present arguments for the scaling form (15) of the exact self-energy and compute asymptotic expressions for the functions $\mathcal{F}_{1,2}(z)$.

Following the same analysis as in Appendix F, we rewrite Eq. (28) as

$$\mathrm{Im}\,\Sigma^{(1),R}_{\boldsymbol{k}}(\omega) = -\frac{2T\omega}{3}\int\frac{d\Omega}{\pi}\int\frac{d^2\boldsymbol{q}}{(2\pi)^2}\frac{[\boldsymbol{k}\times\boldsymbol{q}]^4}{|\boldsymbol{k}+\boldsymbol{q}|^4}\frac{\mathrm{Im}\mathcal{G}^R_{\boldsymbol{q}}(\Omega)}{\Omega(\omega+\Omega)} \times\frac{\mathrm{Im}\Pi^R_{\boldsymbol{q}}(\Omega+\omega)}{|\Pi^R_{\boldsymbol{q}}(\Omega+\omega)|^2}. \tag{G1}$$

Here we use the exact polarization operator and exact Green's function. We use Eqs. (F2) and (44) to rewrite the above expression as

$$\mathrm{Im}\,\Sigma^{(1),R}_{\boldsymbol{k}}(\omega) = -\frac{2\omega\varkappa^2 q_*^{2\eta}}{3\rho}\int\frac{d^2\boldsymbol{q}}{(2\pi)^2}\frac{[\boldsymbol{k}\times\boldsymbol{q}]^4}{|\boldsymbol{k}+\boldsymbol{q}|^{2+2\eta}} \times\int\frac{d\Omega}{\pi}\frac{\mathcal{P}_2\left(\frac{\omega+\Omega}{\omega_{k+q}}\right)}{\left|\mathcal{P}\left(\frac{\omega+\Omega}{\omega_{k+q}}\right)\right|^2(\omega+\Omega)}\frac{\mathcal{A}\left(\frac{\Omega}{\omega_q}\right)}{\omega_q^3}. \tag{G2}$$

In the limit $\omega\to\infty$ we use the fact that integral is dominated by the region $\omega\gg|\Omega|\sim\omega_{\boldsymbol{q}}\sim\omega_{\boldsymbol{k}}$. Therefore, we can use the asymptotic expression for the polarization operator, found in Appendix F,

$$\mathrm{Im}\,\Sigma^{(1),R}_{\boldsymbol{k}}(\omega) \sim -\frac{2\omega\varkappa^2 q_*^{2\eta}}{3\rho}\int\frac{d^2\boldsymbol{q}}{(2\pi)^2}\frac{[\boldsymbol{k}\times\boldsymbol{q}]^4}{|\boldsymbol{k}+\boldsymbol{q}|^{2+2\eta}} \times\left(\frac{\omega}{\omega_{\boldsymbol{k}+\boldsymbol{q}}}\right)^{\gamma}\frac{1}{\omega\omega_{\boldsymbol{q}}^2}\int\frac{dy}{\pi}\mathcal{A}(y), \tag{G3}$$

where $y=\Omega/\omega_q$. In virtue of Eq. (F6), the integral over y converges. Introducing new dimensionless variables $\boldsymbol{q}=k\boldsymbol{r}$ and $\boldsymbol{k}=k\boldsymbol{n}$, we obtain

$$\mathrm{Im}\,\Sigma^{(1),R}_{\boldsymbol{k}}(\omega) \sim \rho\omega\omega_{\boldsymbol{k}}\left(\frac{\omega}{\omega_{\boldsymbol{k}}}\right)^{\gamma-1}\int\frac{d^2\boldsymbol{r}}{(2\pi)^2}\frac{[\boldsymbol{n}\times\boldsymbol{r}]^4}{|\boldsymbol{n}+\boldsymbol{r}|^4 r^{4-\eta}} \times\int\frac{dy}{\pi}\mathcal{A}(y). \tag{G4}$$

Therefore, we reproduce Eq. (50).

In the opposite limit of small frequencies, $\omega\to 0$, we neglect ω under the integral sign in Eq. (G2) and find

$$\mathrm{Im}\,\Sigma^{(1),R}_{\boldsymbol{k}}(\omega) \sim \rho\omega\omega_{\boldsymbol{k}}. \tag{G5}$$

Now using the Kramers-Kroning relations (42), we find at $z\gg 1$

$$\mathcal{F}_1(z) = \mathrm{p.v.}\int_0^\infty\frac{dz}{\pi}\frac{2z^2\mathcal{F}_2(x)}{x^2-z^2}\simeq C_1^{(\infty)}z^{\gamma}, \qquad C_1^{(\infty)} = C_2^{(\infty)}\Phi_\gamma, \tag{G6}$$

where

$$\Phi_\gamma = \mathrm{p.v.}\int_0^\infty\frac{dy}{\pi}\frac{2y^\gamma}{y^2-1} = \int_0^\infty\frac{dt}{\pi t}[(1+t)^\gamma-|1-t|^\gamma]. \tag{G7}$$

Next, applying the Kramers-Kroning relation again, we obtain

$$\mathcal{F}_2(z) = \mathrm{p.v.}\int_0^\infty\frac{dz}{\pi}\frac{2\mathcal{F}_1(x)}{z^2-x^2}\simeq C_1^{\infty}z^{\gamma-1}\Phi_{\gamma-1}. \tag{G8}$$

In order for Eq. (G8) to be mutually consistent with Eq. (50), the function Φ_γ has to satisfy the following relation: $\Phi_\gamma\Phi_{\gamma-1}=-1$. It is indeed the case. Note that $\Phi_{-\gamma}=-\Phi_\gamma$.

The ongoing analysis has demonstrated that the inclusion of self-energy correction in a self-consistent manner yields identical asymptotic outcomes for both the polarization operator and the self-energy. This convergence indicates that universal scaling properties of the exact Green function are reproduced by SCSA-like diagrams. Extending this finding to encompass all correction diagrams requires recognizing a key observation: For every SCSA-like diagram, corresponding non-SCSA-like diagrams exist, characterized by the equivalent number of interaction "wiggly" lines, external momenta, and frequencies. This equivalence stems from the inherent limitation that interaction cannot transmit zero momentum.

Considering the power-law behavior of the self-energy correction in terms of frequency and momentum, instilled by each SCSA-like diagram, the same behavior should be replicated by non-SCSA diagrams. Thus, the distinction lies mainly in numerical factors, with non-SCSA-like diagrams impacting only these specific coefficients.

APPENDIX H: COMPUTATIONS WITHIN $1/d_c$ EXPANSION

In this Appendix we derive asymptotic results for the functions $\mathcal{P}_{1,2}(z)$ and $\mathcal{F}_{1,2}(z)$ within the $1/d_c$ expansion. In order to employ it, we consider 2D membrane embedded into d_c+2-dimensional space. Then $1/d_c$ can serve as the control parameter of the perturbative expansion in the screened interaction [9]. In particular, the bending rigidity exponent η is known to have the following expansion expansion [31]:

$$\eta = \frac{2}{d_c}+\frac{73-68\zeta(3)}{27d_c^2}+\ldots. \tag{H1}$$

Consequently, from Eq. (32) we find the following expansion for the exponent γ:

$$\gamma = 1-\frac{3}{2d_c}-\frac{25-17\zeta(3)}{9d_c^2}+\ldots \tag{H2}$$

In Appendix F we derived the exact form of the polarization operator. For its imaginary part we obtained the asymptotic expressions (45) and (46). In the limit $d_c\to\infty$ we can express $P_{1,2}(z)$ as a series expansion in terms of $1/d_c$. For example, for $z\gg 1$, we find

$$P_1(z) = B_1^{(\infty)}z^{-\gamma} = \left[B_{1,0}^{(\infty)}+\frac{1}{d_c}B_{1,1}^{(\infty)}+\ldots\right] \times\frac{1}{z}\left(1+\frac{3}{2d_c}\ln|z|+\ldots\right) \tag{H3}$$

and similar expression for $P_2(z)$.

Since $1/d_c$ is a perturbation parameter, we can derive coefficients $B_{2,0}^{(\infty)}$ and $B_{2,0}^{(0)}$ by simply considering polarization operator, consisting of "bare" Green's functions. Thus, for the

imaginary part we obtain

$$\mathrm{Im}\Pi_{\boldsymbol{q}}^{(0),R}(\Omega)=\frac{2d_cT\Omega}{3}\int\frac{d\omega}{2\pi}\int\frac{d^2\boldsymbol{k}}{(2\pi)^2}\frac{[\boldsymbol{k}\times\boldsymbol{q}]^4}{q^4}\frac{\mathrm{Im}G_{\boldsymbol{k}}^R(\omega)}{\omega}\times\frac{\mathrm{Im}G_{\boldsymbol{k}+\boldsymbol{q}}^R(\omega+\Omega)}{\omega+\Omega},\tag{H4}$$

where the imaginary part of "bare" Green's function is given by (A3). Performing integrals over frequency ω and momentum $\boldsymbol{k}$, we derive

$$\mathrm{Im}\Pi_{\boldsymbol{q}}^{(0),R}(\Omega)=\frac{T}{\varkappa^2q^2}\mathcal{P}_2^{(0),0}\left(\frac{\Omega}{\omega_q}\right).\tag{H5}$$

Here the function $\mathcal{P}_2^{(0),0}(z)$ is odd, and for $z>0$ it is given as

$$\mathcal{P}_2^{(0),0}(z)=\frac{d_cz}{96}\begin{cases}1, & z<\frac{1}{2},\\ 1+\dfrac{(1-2z)^2(z+1)}{2z^3}, & \frac{1}{2}\leqslant z<1,\\ \dfrac{(3z+1)}{2z^3}, & 1\leqslant z.\end{cases}\tag{H6}$$

We use Eq. (H6) in order to derive the expansion of the coefficients $B_2^{(0)}$ and $B_2^{(\infty)}$ in powers $1/d_c$. In particular, we obtain

$$B_2^{(0)}=\frac{d_c}{96}+O(1),\quad B_2^{(\infty)}=\frac{d_c}{64}+O(1).\tag{H7}$$

In order to find the expansion for the coefficients $B_1^{(0)}$ and $B_1^{(\infty)}$, we need to compute the real part of the retarded polarization operator at finite frequency. With the help of the Kramers-Kronig relation, we find

$$\mathrm{Re}\Pi_{\boldsymbol{q}}^{(0),R}(\Omega)=\mathrm{p.v.}\int_{-\infty}^{\infty}\frac{d\omega}{\pi}\frac{\mathrm{Im}\Pi_{\boldsymbol{q}}^{(0),R}(\omega)}{\omega-\Omega}=\frac{T}{\varkappa^2q^2}\mathcal{P}_1^{(0),0}\left(\frac{\Omega}{\omega_q}\right),\tag{H8}$$

where the even function $\mathcal{P}_1^{(0),0}(z)$ is given explicitly as

$$\mathcal{P}_1^{(0),0}(z)=\frac{d_c}{192\pi z^2}\Big[(2z+1)^2(z-1)\ln|1+2z|+8z^2-(2z-1)^2(z+1)\ln|1-2z|+6z(1-z^2)\ln\left|\frac{1+z}{1-z}\right|\Big].\tag{H9}$$

Expanding $\mathcal{P}_1^{(0),0}(z)$ in series in powers of z, we obtain

$$\mathcal{P}_1^{(0),0}(0)=\frac{d_c}{16\pi}+O(1),\quad B_1^{(0)}=O(1).\tag{H10}$$

Next, expanding at $z\gg1$ we derive $P_1^{(0),0}(z)\sim-d_cz^{-2}\ln z$. We see that it is a subleading contribution as one can see from Eq. (H3). Therefore, in order to find $B_1^{(\infty)}$, straightforward usage of the result (H9) is not possible. Instead we apply the relation (48) and the following asymptotic expression for the function Φ_γ:

$$\Phi_{1-\alpha}\simeq\frac{2}{\pi\alpha},\quad\alpha\ll1.\tag{H11}$$

Then we derive the following result:

$$B_1^{(\infty)}=-\frac{d_c^2}{96\pi}+O(d_c).\tag{H12}$$

A similar procedure can be employed for the imaginary part of the self-energy correction. Let us consider the lowest order (in $1/d_c$) correction,

$$\mathrm{Im}\Sigma_{\boldsymbol{k}}^{(1),R}(\omega)=\frac{2T\omega}{3}\int\frac{d\Omega}{\pi}\int\frac{d^2\boldsymbol{q}}{(2\pi)^2}\frac{[\boldsymbol{k}\times\boldsymbol{q}]^4}{q^4}\frac{\mathrm{Im}\Pi_{\boldsymbol{q}}^{(0),R}(\Omega)}{\left|\Pi_{\boldsymbol{q}}^{(0),R}(\Omega)\right|^2}\times\frac{\mathrm{Im}G_{\boldsymbol{k}+\boldsymbol{q}}^R(\omega+\Omega)}{\Omega(\omega+\Omega)}.\tag{H13}$$

Substituting (A4) into (H13) and integrating over frequency, we obtain

$$\mathrm{Im}\Sigma_{\boldsymbol{k}}^{(1),R}(\omega)=\frac{T\omega}{3\rho}\int\frac{d^2\boldsymbol{q}}{(2\pi)^2}\frac{[\boldsymbol{k}\times\boldsymbol{q}]^4}{q^4}\times\sum_{s=\pm1}\frac{1}{\omega_{\boldsymbol{q}+\boldsymbol{k}}^{(0)2}\left(\omega+s\omega_{\boldsymbol{q}+\boldsymbol{k}}^{(0)}\right)}\frac{\mathrm{Im}\Pi_{\boldsymbol{q}}^{(0),R}\left(\omega+s\omega_{\boldsymbol{q}+\boldsymbol{k}}^{(0)}\right)}{\left|\Pi_{\boldsymbol{q}}^{(0),R}\left(\omega+s\omega_{\boldsymbol{q}+\boldsymbol{k}}^{(0)}\right)\right|^2}.\tag{H14}$$

In the limit $\omega\ll\omega_{\boldsymbol{k}}$ we can neglect the external frequency ω under the integral sign and obtain

$$\mathrm{Im}\Sigma_{\boldsymbol{k}}^{(1),R}(\omega)=\frac{2T\omega}{3\rho}\int\frac{d^2\boldsymbol{q}}{(2\pi)^2}\frac{[\boldsymbol{k}\times\boldsymbol{q}]^4}{q^4\omega_{\boldsymbol{q}+\boldsymbol{k}}^{(0)3}}\frac{\mathrm{Im}\Pi_{\boldsymbol{q}}^{(0),R}\left(\omega_{\boldsymbol{q}+\boldsymbol{k}}^{(0)}\right)}{\left|\Pi_{\boldsymbol{q}}^{(0),R}\left(\omega_{\boldsymbol{q}+\boldsymbol{k}}^{(0)}\right)\right|^2}.\tag{H15}$$

Then with the help of Eqs. (H6) and (H9) the integral over $\boldsymbol{q}$ can be evaluated numerically. Hence, for $\omega\ll\omega_{\boldsymbol{k}}$ we obtain

$$\mathrm{Im}\Sigma_{\boldsymbol{k}}^{(1),R}(\omega)\approx1.57\frac{\rho\omega\omega_k}{d_c}.\tag{H16}$$

Using the above asymptotic result, we find

$$\mathcal{F}_2(0)=\frac{1.57}{d_c}+O\left(\frac{1}{d_c^2}\right).\tag{H17}$$

In order to determine asymptotics in the opposite limit, $\omega\gg\omega_{\boldsymbol{k}}$, we neglect $\omega_{\boldsymbol{q}+\boldsymbol{k}}$ in comparison with ω under the integral sign. Then we find

$$\mathrm{Im}\Sigma_{\boldsymbol{k}}^{(1),R}(\omega)=\frac{2T}{3\rho}\int\frac{d^2\boldsymbol{q}}{(2\pi)^2}\frac{[\boldsymbol{k}\times\boldsymbol{q}]^4}{q^4\omega_{\boldsymbol{q}+\boldsymbol{k}}^{(0)2}}\frac{\mathrm{Im}\Pi_{\boldsymbol{q}}^{(0),R}(\omega)}{\left|\Pi_{\boldsymbol{q}}^{(0),R}(\omega)\right|^2}.\tag{H18}$$

We proceed by substituting Eqs. (H5) and (H8) into the above expression. It is convenient to introduce new variables $\boldsymbol{k}=k\boldsymbol{n}$, $\boldsymbol{q}=k\boldsymbol{r}$, $z=\omega/\omega_{\boldsymbol{k}}$. Then we obtain

$$\mathrm{Im}\Sigma_{\boldsymbol{k}}^{(1),R}(\omega)=\frac{2}{3d_c}\rho\omega_{\boldsymbol{k}}^2\int\frac{d^2\boldsymbol{r}}{(2\pi)^2}\frac{[\boldsymbol{n}\times\boldsymbol{r}]^4}{r^2|\boldsymbol{r}+\boldsymbol{n}|^4}\times\frac{\mathcal{P}_2^{(0),0}\left(z/r^2\right)}{\left[\mathcal{P}_1^{(0),0}(z/r^2)\right]^2+\left[\mathcal{P}_2^{(0),0}(z/r^2)\right]^2}.\tag{H19}$$

In the limit $z\gg1$ we can use asymptotic expressions for $\mathcal{P}_2^{(0),0}(z)$ and $\mathcal{P}_1^{(0),0}(z)$ [see Eqs. (H6) and (H9)] since the

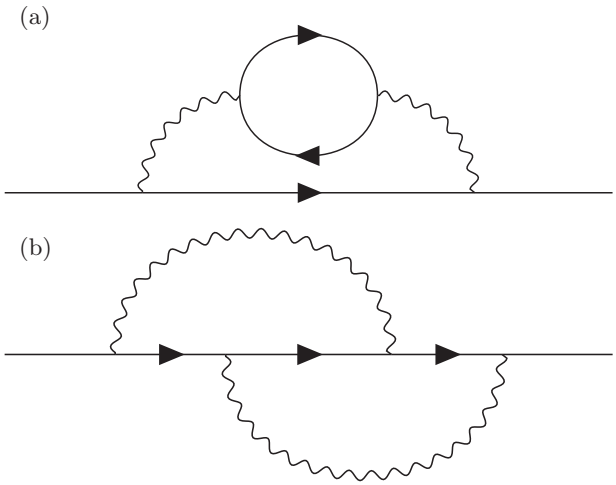

FIG. 10. Diagrams for self-energy in the second order of interaction with nonzero imaginary part.

integral is dominated by $r \ll \sqrt{z}$. Thus, we obtain

$$\mathrm{Im}\,\Sigma_{\boldsymbol{k}}^{(1),R}(\omega) = \frac{32z}{3d_c\pi^2}\rho\omega_{\boldsymbol{k}}^2 \int_0^\infty r dr \int_0^{2\pi} \frac{d\varphi\ \sin^4\varphi}{(r^2+1+2r\cos\varphi)^2}. \tag{H20}$$

The integral over angle φ can be easily evaluated:

$$\int_0^{2\pi} d\varphi \frac{\sin^4\varphi}{(r^2+1+2r\cos\varphi)^2} = \frac{3\pi}{4}\begin{cases}1, & r\leqslant 1,\\ r^{-4}, & r>1.\end{cases} \tag{H21}$$

Finally, we obtain the asymptotic expression

$$\mathrm{Im}\,\Sigma_{\boldsymbol{k}}^{(1),R}(\omega) \simeq \frac{8}{\pi d_c}\rho\omega\omega_{\boldsymbol{k}}, \quad \omega \gg \omega_{\boldsymbol{k}}. \tag{H22}$$

Using the above expression, we derive

$$C_2^{(\infty)} = \frac{8}{\pi d_c} + O\left(\frac{1}{d_c^2}\right). \tag{H23}$$

In order to find the expansion of $C_1^{(\infty)}$ we use the relation (51). Then using Eq. (H11), we find

$$C_1^{(\infty)} = \frac{32}{3\pi^2} + O\left(\frac{1}{d_c}\right). \tag{H24}$$

APPENDIX I: CALCULATION OF THE IMAGINARY PART OF THE SELF-ENERGY BEYOND THE UNIVERSAL REGIME

We have shown that in the region $q \gg q_*$ or $\Omega \gg \omega_*$ screening of the interaction is negligible in virtue of the condition $Y\Pi_q(\Omega) \ll 1$. Therefore, we could calculate decay rate for flexural phonons in this regime using perturbation theory.

In the first order in interaction the correction to the self-energy is real. Thus, in order to calculate the attenuation, we need to study the second-order corrections. There are two diagrams in that order with nonzero imaginary part (see Fig. 10). In this Appendix we will the present results for the diagram (a) only since the diagram with crossed lines (b) is of the same or smaller magnitude.

We start from the following expression:

$$\mathrm{Im}\,\Sigma_{\boldsymbol{k}}^{(a),R}(\omega) \sim TY^2\omega \int d\Omega \int d^2\boldsymbol{q} \frac{[\boldsymbol{k}\times\boldsymbol{q}]^4}{q^4} \frac{\mathrm{Im}\,\Pi_{\boldsymbol{q}}^R(\Omega)}{\Omega} \times \frac{\mathrm{Im}\,G_{\boldsymbol{q}+\boldsymbol{k}}^R(\omega+\Omega)}{\omega+\Omega}. \tag{I1}$$

We first consider the case $k \gg q_*$ (regions II_b and III in Fig. 2). Making the integral dimensionless, we obtain

$$\mathrm{Im}\,\Sigma_{\boldsymbol{k}}^{(a),R}(\omega) = \left(\frac{q_*}{k}\right)^4 \rho\omega\omega_{\boldsymbol{k}} f_2^{(a)}(z), \tag{I2}$$

where $z = \omega/\omega_{\boldsymbol{k}}$ and $\omega_{\boldsymbol{k}} = Dk^2$. After straightforward calculations we obtain asymptotics

$$f_2^{(a)}(z) \sim \begin{cases}\text{const}, & |z| \ll 1,\\ 1/z^2, & |z| \gg 1.\end{cases} \tag{I3}$$

Therefore, in the regime $k \gg q_*$, we find

$$\mathrm{Im}\,\Sigma_{\boldsymbol{k}}^{(a),R}(\omega) \sim \left(\frac{\omega_*}{\max\{\omega,\omega_{\boldsymbol{k}}\}}\right)^2 \rho\omega\omega_{\boldsymbol{k}}. \tag{I4}$$

This form suggests that the obtained correction is small in virtue of a small parameter $q_*/k \ll 1$ that controls the perturbation theory.

In the region $k \ll q_*$ and $\omega \gg \omega_*$ (region II_a in Fig. 2), we need to account for renormalization of the bending rigidity. Thus we obtain

$$\mathrm{Im}\,\Sigma_{\boldsymbol{k}}^{(a),R}(\omega) \sim \frac{T^2Y^2\omega}{\varkappa^2} \int d^2\boldsymbol{q} \frac{[\boldsymbol{k}\times\boldsymbol{q}]^4}{|\boldsymbol{k}+\boldsymbol{q}|^6} \frac{1}{\rho\omega_{\boldsymbol{q}}^2} \times \sum_{s\pm1} \mathcal{P}_2\left(\frac{\omega+s\omega_{\boldsymbol{q}}}{D|\boldsymbol{k}+\boldsymbol{q}|^2}\right) \frac{1}{\omega+s\omega_{\boldsymbol{q}}}. \tag{I5}$$

The integral over momentum is dominated by $q \sim k$, and, therefore, we have to use $\omega_{\boldsymbol{q}} = Dq^{2-\eta/2}q_*^{\eta/2}$. Evaluating the integral over q, we find

$$\mathrm{Im}\,\Sigma_{\boldsymbol{k}}^{(a),R}(\omega) \sim \rho\omega_*^2\left(\frac{k}{q_*}\right)^\eta \frac{Dk^2}{\omega}. \tag{I6}$$

Special care is needed for calculation of the imaginary part of the self-energy at the mass shell $\omega = \omega_{\boldsymbol{k}} \gg \omega_*$. As one can see, the following contribution:

$$\mathrm{Im}\,\Sigma_{\boldsymbol{k}}^{(a),R}(\omega) \sim \frac{T^2Y^2\omega}{\varkappa^2} \int d^2\boldsymbol{q} \frac{[\boldsymbol{k}\times\boldsymbol{q}]^4}{q^6} \times \mathcal{P}_2\left(\frac{\omega_{\boldsymbol{k}+\boldsymbol{k}}-\omega_{\boldsymbol{k}}}{\omega_{\boldsymbol{q}}}\right) \frac{1}{\rho\omega_{\boldsymbol{q}}^2} \frac{1}{\omega_{\boldsymbol{k}+\boldsymbol{q}}-\omega_{\boldsymbol{k}}} \tag{I7}$$

diverges due to singularity at $q \to 0$. To fix this problem, one has to work with the full RPA screened interaction. Then we obtain

$$\mathrm{Im}\,\Sigma_{\boldsymbol{k}}^{(a),R}(\omega) \sim T\omega_{\boldsymbol{k}} \int d^2\boldsymbol{q} \frac{Y^2\mathrm{Im}\,\Pi_{\boldsymbol{q}}^R(\omega_{\boldsymbol{k}+\boldsymbol{q}}-\omega_{\boldsymbol{k}})}{\left|1+3Y\Pi_{\boldsymbol{q}}^R(\omega_{\boldsymbol{k}+\boldsymbol{q}}-\omega_{\boldsymbol{k}})/2\right|^2} \times \frac{1}{\rho\omega_{\boldsymbol{k}+\boldsymbol{q}}^2} \frac{[\boldsymbol{k}\times\boldsymbol{q}]^4}{q^4} \frac{1}{\omega_{\boldsymbol{k}}-\omega_{\boldsymbol{k}+\boldsymbol{q}}}. \tag{I8}$$

The integral over q is now dominated by $q \sim q_*$ rather than $q = 0$. This justifies the usage of the full form of the RPA

screened interaction. Using asymptotics for the imaginary part of the polarization operator, Eq. (46), we obtain final result

$$\mathrm{Im}\,\Sigma_{\boldsymbol{k}}^{(a),R}(\omega) \sim \rho\omega_*^2 \frac{k}{q_*}. \tag{I9}$$

This result is valid for $|\omega - Dk^2| \ll \omega_*$ since in that region integral over q is also dominated by $q \sim q_*$ and the same approximations have to be employed.

[1] K. S. Novoselov, A. K. Geim, S. V. Morozov, D. Jiang, Y. Zhang, S. V. Dubonos, I. V. Grigorieva, and A. A. Firsov, Electric field effect in atomically thin carbon films, Science **306**, 666 (2004).

[2] K. S. Novoselov, A. K. Geim, S. V. Morozov, D. Jiang, M. I. Katsnelson, I. V. Grigorieva, S. V. Dubonos, and A. A. Firsov, Two-dimensional gas of massless Dirac fermions in graphene, Nature (Lond.) **438**, 197 (2005).

[3] Y. Zhang, Y.-W. Tan, H. L. Stormer, and P. Kim, Experimental observation of the quantum Hall effect and Berry's phase in graphene, Nature (Lond.) **438**, 201 (2005).

[4] K. S. Novoselov and A. H. C. Neto, Two-dimensional crystals-based heterostructures: Materials with tailored properties, Phys. Scr. **2012**, 014006 (2012).

[5] P. Avouris, T. F. Heinz, and T. Low (eds.), *2D Materials: Properties and Devices* (Cambridge University Press, Cambridge, UK, 2017).

[6] D. Nelson and L. Peliti, Fluctuations in membranes with crystalline and hexatic order, J. Phys. France **48**, 1085 (1987).

[7] J. A. Aronovitz and T. C. Lubensky, Fluctuations of solid membranes, Phys. Rev. Lett. **60**, 2634 (1988).

[8] M. Paczuski, M. Kardar, and D. R. Nelson, Landau theory of the crumpling transition, Phys. Rev. Lett. **60**, 2638 (1988).

[9] F. David and E. Guitter, Crumpling transition in elastic membranes: Renormalization group treatment, Europhys. Lett. **5**, 709 (1988).

[10] J. Aronovitz, L. Golubovic, and T. C. Lubensky, Fluctuations and lower critical dimensions of crystalline membranes, J. Phys. France **50**, 609 (1989).

[11] E. Guitter, F. David, S. Leibler, and L. Peliti, Crumpling and buckling transitions in polymerized membranes, Phys. Rev. Lett. **61**, 2949 (1988).

[12] E. Guitter, F. David, S. Leibler, and L. Peliti, Thermodynamical behavior of polymerized membranes, J. Phys. France **50**, 1787 (1989).

[13] J. Toner, Elastic anisotropies and long-ranged interactions in solid membranes, Phys. Rev. Lett. **62**, 905 (1989).

[14] P. Le Doussal and L. Radzihovsky, Self-consistent theory of polymerized membranes, Phys. Rev. Lett. **69**, 1209 (1992).

[15] D. C. Morse, T. C. Lubensky, and G. S. Grest, Quenched disorder intethered membranes, Phys. Rev. A **45**, R2151(R) (1992).

[16] D. R. Nelson and L. Radzihovsky, Polymerized membranes with quenched random internal disorder, Europhys. Lett. **16**, 79 (1991).

[17] L. Radzihovsky and D. R. Nelson, Statistical mechanics of randomly polymerized membranes, Phys. Rev. A **44**, 3525 (1991).

[18] D. C. Morse and T. C. Lubensky, Curvature disorder in tethered membranes: A new flat phase at $t = 0$, Phys. Rev. A **46**, 1751 (1992).

[19] D. Bensimon, D. Mukamel, and L. Peliti, Quenched curvature disorder in polymerized membranes, Europhys. Lett. **18**, 269 (1992).

[20] L. Radzihovsky and J. Toner, A new phase of tethered membranes: Tubules, Phys. Rev. Lett. **75**, 4752 (1995).

[21] L. Radzihovsky and J. Toner, Elasticity, shape fluctuations, and phase transitions in the new tubule phase of anisotropic tethered membranes, Phys. Rev. E **57**, 1832 (1998).

[22] E. I. Kats and V. V. Lebedev, Asymptotic freedom at zero temperature in free-standing crystalline membranes, Phys. Rev. B **89**, 125433 (2014).

[23] I. V. Gornyi, V. Y. Kachorovskii, and A. D. Mirlin, Rippling and crumpling in disordered free-standing graphene, Phys. Rev. B **92**, 155428 (2015).

[24] E. I. Kats and V. V. Lebedev, Erratum: Asymptotic freedom at zero temperature in free-standing crystalline membranes [Phys. Rev. B 89, 125433 (2014)], Phys. Rev. B **94**, 079904 (2016).

[25] I. S. Burmistrov, I. V. Gornyi, V. Y. Kachorovskii, M. I. Katsnelson, and A. D. Mirlin, Quantum elasticity of graphene: Thermal expansion coefficient and specific heat, Phys. Rev. B **94**, 195430 (2016).

[26] I. V. Gornyi, V. Y. Kachorovskii, and A. D. Mirlin, Anomalous Hooke's law in disordered graphene, 2D Mater. **4**, 011003 (2016).

[27] A. Košmrlj and D. R. Nelson, Statistical mechanics of thin spherical shells, Phys. Rev. X **7**, 011002 (2017).

[28] P. Le Doussal and L. Radzihovsky, Anomalous elasticity, fluctuations and disorder in elastic membranes, Ann. Phys. **392**, 340 (2018).

[29] I. S. Burmistrov, V. Y. Kachorovskii, I. V. Gornyi, and A. D. Mirlin, Differential Poisson's ratio of a crystalline two-dimensional membrane, Ann. Phys. **396**, 119 (2018).

[30] I. S. Burmistrov, I. V. Gornyi, V. Y. Kachorovskii, M. I. Katsnelson, J. H. Los, and A. D. Mirlin, Stress-controlled Poisson ratio of a crystalline membrane: Application to graphene, Phys. Rev. B **97**, 125402 (2018).

[31] D. Saykin, I. Gornyi, V. Kachorovskii, and I. Burmistrov, Absolute Poisson's ratio and the bending rigidity exponent of a crystalline two-dimensional membrane, Ann. Phys. **414**, 168108 (2020).

[32] D. R. Saykin, V. Y. Kachorovskii, and I. S. Burmistrov, Phase diagram of a flexible two-dimensional material, Phys. Rev. Res. **2**, 043099 (2020).

[33] O. Coquand, D. Mouhanna, and S. Teber, The flat phase of polymerized membranes at two-loop order, Phys. Rev. E **101**, 062104 (2020).

[34] A. Mauri and M. I. Katsnelson, Scaling behavior of crystalline membranes: An ε-expansion approach, Nucl. Phys. B **956**, 115040 (2020).

[35] A. Mauri and M. I. Katsnelson, Scale without conformal invariance in membrane theory, Nucl. Phys. B **969**, 115482 (2021).

[36] P. Le Doussal and L. Radzihovsky, Thermal buckling transition of crystalline membranes in a field, Phys. Rev. Lett. **127**, 015702 (2021).

[37] S. Shankar and D. R. Nelson, Thermalized buckling of isotropically compressed thin sheets, Phys. Rev. E **104**, 054141 (2021).
[38] A. Mauri and M. I. Katsnelson, Perturbative renormalization and thermodynamics of quantum crystalline membranes, Phys. Rev. B **105**, 195434 (2022).
[39] S. Metayer, D. Mouhanna, and S. Teber, Three-loop order approach to flat polymerized membranes, Phys. Rev. E **105**, L012603 (2022).
[40] I. S. Burmistrov, V. Y. Kachorovskii, M. J. Klug, and J. Schmalian, Emergent continuous symmetry in anisotropic flexible two-dimensional materials, Phys. Rev. Lett. **128**, 096101 (2022).
[41] M. V. Parfenov, V. Y. Kachorovskii, and I. S. Burmistrov, Disorder-driven transition to tubular phase in anisotropic two-dimensional materials, Phys. Rev. B **106**, 235415 (2022).
[42] V. V. Lebedev and E. I. Kats, Long-scale dynamics of crystalline membranes, Phys. Rev. B **85**, 045416 (2012).
[43] K. Mizuochi, H. Nakanishi, and T. Sakaue, Dynamical scaling of polymerized membranes, Europhys. Lett. **107**, 38003 (2014).
[44] E. Granato, M. Greb, K. R. Elder, S. C. Ying, and T. Ala-Nissila, Dynamic scaling of out-of-plane fluctuations in freestanding graphene, Phys. Rev. B **105**, L201409 (2022).
[45] E. Granato, K. R. Elder, S. C. Ying, and T. Ala-Nissila, Dynamics of fluctuations and thermal buckling in graphene from a phase-field crystal model, Phys. Rev. B **107**, 035428 (2023).
[46] C. Steinbock and E. Katzav, Thermally driven elastic membranes are quasi-linear across all scales, J. Phys. A: Math. Theor. **56**, 215002 (2023).
[47] J. Li, J. Li, J. Tang, Z. Tao, S. Xue, J. Liu, H. Peng, X.-Q. Chen, J. Guo, and X. Zhu, Direct observation of topological phonons in graphene, Phys. Rev. Lett. **131**, 116602 (2023).
[48] T. Miao, S. Yeom, P. Wang, B. Standley, and M. Bockrath, Graphene nanoelectromechanical systems as stochastic-frequency oscillators, Nano Lett. **14**, 2982 (2014).
[49] R. van Leeuwen, A. Castellanos-Gomez, G. A. Steele, H. S. J. van der Zant, and W. J. Vestra, Time-domain response of atomically thin MoS_2 nanomechanical resonators, Appl. Phys. Lett. **105**, 041911 (2014).
[50] P. G. Steeneken, R. J. Dolleman, D. Davidovik, F. Alijani, and H. S. J. van der Zant, Dynamics of 2D material membranes, 2D Mater. **8**, 042001 (2021).
[51] P. F. Ferrari, S. Kim, and A. V. van der Zande, Nanoelectromechanical systems from two-dimensional materials, Appl. Phys. Rev. **10**, 031302 (2023).
[52] M. L. Ackerman, P. Kumar, M. Neek-Amal, P. M. Thibado, F. M. Peeters, and S. Singh, Anomalous dynamical behavior of freestanding graphene membranes, Phys. Rev. Lett. **117**, 126801 (2016).
[53] C. Seoánez, F. Guinea, and A. H. Castro Neto, Dissipation in graphene and nanotube resonators, Phys. Rev. B **76**, 125427 (2007).
[54] A. Tröster, Fourier Monte Carlo simulation of crystalline membranes in the flat phase, J. Phys.: Conf. Ser. **454**, 012032 (2013).
[55] A. Croy, D. Midtvedt, A. Isacsson, and J. M. Kinaret, Nonlinear damping in graphene resonators, Phys. Rev. B **86**, 235435 (2012).
[56] S. De, A. van der Zande, and N. R. Aluru, Intrinsic dissipation due to mode coupling in two-dimensional-material resonators revealed through a multiscale approach, Phys. Rev. Appl. **14**, 034062 (2020).
[57] L. Radzihovsky and P. Le Doussal, Crumpled glass phase of randomly polymerized membranes in the large d limit, J. Phys. I **2**, 599 (1992).
[58] A. D. Kokovin, V. Yu. Kachorovskii, and I. S. Burmistrov, companion paper, Narrowing of the flexural phonon spectral line in stressed crystalline two-dimensional materials, Phys. Rev. Lett. **133**, 136203 (2024).
[59] A. Bachtold, K. Moser, and M. I. Dykman, Mesoscopic physics of nanomechanical systems, Rev. Mod. Phys. **94**, 045005 (2022).